Running title: Functional diversification in COPII gene families

The COPII components Sec23 and Sec24 form isoform specific subcomplexes with Sec23D/E and Sec24C/D essential for tip growth

Mingqin Chang[1,2,3], Shu-Zon Wu[1], Jacquelyn E. O'Sullivan[4,5] and Magdalena Bezanilla[1]*

[1] Department of Biological Sciences, Dartmouth College, Hanover, NH 03755
[2] Plant Biology Graduate Program, University of MA Amherst, Amherst, MA 01002
[3] Current address: Department of Plant Sciences, UC Davis, Davis, CA 95616
[4] Department of Biology, University of MA Amherst, Amherst, MA 01002
[5] Current address: Tufts School of Medicine, Boston, MA 02111

*Corresponding author
email: magdalena.bezanilla@dartmouth.edu

The author responsible for distribution of materials integral to the findings presented in this article in accordance with the policy described in the Instructions for Authors (www.plantcell.org) is: Magdalena Bezanilla (magdalena.bezanilla@dartmouth.edu).

Abstract

COPII, a coat of proteins that form vesicles on the ER, mediates vesicle traffic from the ER to the Golgi. In contrast to metazoans that have few genes encoding each COPII component, plants have expanded these gene families leading to the hypothesis that plant COPII has functionally diversified. Here, we analyzed the gene families encoding for the Sec23/24 heterodimer in the moss *Physcomitrium (Physcomitrella) patens*. In *P. patens*, *Sec23* and *Sec24* gene families are each comprised of seven genes. We discovered that *Sec23D* is functionally redundant with *Sec23E* and together they are essential for protonemal development. Sec23D is critical for secretion to the Golgi and the plasma membrane in tip growing protonemata. Sec23D preferentially associates with Sec24C/D, also essential for protonemata. In contrast, the remaining five *Sec23* genes are dispensable for tip growth, but are redundant with *Sec23D/E* for gametophore formation. While *Sec23A/B/C/F/G* do not quantitatively affect Golgi secretion in protonemata, they do contribute to secretion to the plasma membrane. Furthermore, the three highly expressed *Sec23* genes in protonemata, *Sec23B/D/G* form morphologically distinct ER exit sites. These data suggest that *Sec23D/E* form unique ER exit sites contributing to secretion that is essential for tip growing protonemata.

50 **Introduction**

51 Trafficking from the ER to the Golgi is mediated by the Coat Protein
52 complex II (COPII). COPII facilitates the formation of transport vesicles at ER exit
53 sites promoting the delivery of cargo, including transmembrane proteins, soluble
54 proteins and lipids, to *cis*-Golgi compartments (Brandizzi and Barlowe,
55 2013)(Barlowe and Helenius, 2016) (Aridor, 2018)(Hanna et al., 2018). The
56 COPII coat comprises two layers of protein complexes. The inner layer consists
57 of a Sar1-Sec23-Sec24 lattice, while the outer layer is made up of Sec31-Sec13
58 heterotetramers (Stagg et al., 2008; Whittle and Schwartz, 2010; Bi et al., 2002;
59 Fath et al., 2007). Sar1 is a small GTPase of the Ras super family that is the
60 master regulator of COPII vesicle biogenesis (Nakano and Muramatsu, 1989).
61 Assembly of COPII coat is initiated by the conversion of Sar1-GDP to Sar1-GTP,
62 which is mediated by Sec12, a guanine nucleotide exchange factor (GEF) that is
63 an ER resident membrane protein (Barlowe and Schekman, 1993; Nakano and
64 Muramatsu, 1989). At the ER surface, activated Sar1 recruits the Sec23-Sec24
65 heterodimer, which associates with the ER membrane as an "inner coat". The
66 Sar1-Sec23-Sec24-cargo "pre-budding" complex in turn recruits the Sec13-Sec31
67 heterotetramer, referred to as an "outer coat" to the nascent bud (Aridor et al.,
68 1998; Salama et al.). The polymerization of Sec13-Sec31 heterotetramers
69 induces membrane curvature and completes vesicle biogenesis (Fath et al., 2007;
70 Stagg et al., 2006; Whittle and Schwartz, 2010).

71 Selective recruitment of cargos into COPII coated vesicles is driven by ER
72 export signals located on cytoplasmically exposed regions of cargo proteins
73 (Barlowe, 2003). ER export signals of most transmembrane cargo proteins are
74 thought to interact directly with the inner coat components of COPII. However,
75 some transmembrane and most soluble cargo proteins interact with COPII
76 components through ER-resident transmembrane adaptors or receptors
77 (Barlowe, 2003). Sec24 is the COPII component that has been implicated in
78 recognizing these various sorting signals (Mossessova et al., 2003; Nufer, 2003).
79 However, several studies suggested that Sec23 and Sar1 may also play roles in
80 cargo sorting by directly binding to the export signals (Aridor et al., 2001;
81 Mancias and Goldberg, 2007; Giraudo and Maccioni, 2003).

82 Based on the high sequence similarity among COPII paralogs, and cross-
83 species complementation studies (De Craene et al., 2014; Khoriaty et al., 2018) it
84 is assumed that functions of COPII components are conserved across eukaryotes.
85 While components of the COPII coat are well studied in budding yeast and
86 mammalian cells, illustrating their molecular functions in plants has been more
87 challenging. Comparative genomic analyses revealed that gene families encoding
88 COPII components have undergone gene expansions in plants with Sec23
89 exhibiting the largest expansion (Aridor et al., 2001; Mancias and Goldberg,
90 2007; Giraudo and Maccioni, 2003). While there are only one and two Sec23
91 genes in *S. cerevisiae* and mammals (eg. mice and humans) (Jensen and
92 Schekman, 2011), respectively, there are seven in both *P. patens* and *A. thaliana*
93 (Brandizzi, 2018). Since Sec23 and its heterodimeric partner Sec24 are
94 implicated in cargo sorting, the larger Sec23 gene family could suggest that
95 plants have more diverse sorting signals requiring specificity at the level of the
96 Sec23/Sec24 heterodimer. Consistent with this, in contrast to yeast, which has a
97 single gene for most COPII components, all other components of COPII in plants
98 are encoded by multiple genes, suggesting that cargo specificity may translate to
99 formation of distinct COPII complexes and vesicle populations. Alternatively,
100 larger gene families could simply indicate that plants have higher functional
101 redundancy in COPII encoded gene families.
102 Genetic studies in *A. thaliana* have demonstrated that loss of specific
103 COPII components caused developmental defects. A complete knockout of
104 AtSec24A was lethal (Faso et al., 2009; Nakano et al., 2009). However, a missense
105 point mutation in AtSec24A (R693K) resulted in ER morphology defects and
106 disruption of ER-Golgi integrity. Interestingly, these phenotypes could not be
107 rescued by either AtSec24B or AtSec24C (Faso et al., 2009; Nakano et al., 2009),
108 suggesting that AtSec24B and C are functionally distinct from AtSec24A. Even
109 though AtSec24B and AtSec24C did not rescue the *Atsec24a* missense mutant
110 and each were not important for plant viability, they were shown to influence the
111 development of reproductive cells (Tanaka et al., 2013). Functional
112 diversification was also suggested by analysis of AtSec16 mutants in which
113 storage protein precursors were accumulated abnormally in *Atsec16a* null
114 mutants, but not in *Atsec16b* null mutants (Takagi et al., 2013).

While *P. patens* and *A. thaliana* have similar numbers of genes encoding COPII components, moss has several attributes that make it particularly suited to study COPII function. *P. patens* juvenile tissues are haploid and comprise multiple tissue types that establish the plant body. Protonemal tissue, which emerges from the spore and is also readily propagated vegetatively by tissue homogenization, is composed of tip-growing cells constituting a two-dimensional filamentous network. The predictable patterns of growth and cell division provide an easily tractable system for analysis of mutant phenotypes. As a single-cell-layer, protonemal tissue also enables high-resolution microscopy of endogenously tagged fluorescent proteins in live cells (Rensing et al., 2020). In addition to amenable tissue morphology and haploid lifestyle, *P. patens* exhibits high rates of efficient homologous recombination and CRISPR Cas9-mediated genome editing (Rensing et al., 2020)r. Here, we utilized these molecular genetic and live-cell imaging tools to systematically characterize the *Sec23* gene family. Analysis of mutant phenotypes and protein localization revealed a high degree of functional specificity among Sec23 isoforms, differentially influencing secretion to the Golgi and the plasma membrane as well as the size of presumptive ER exit sites. We also found that Sec23D only forms heterodimers with a subset of Sec24 isoforms, suggesting that COPII complexes may have fixed isoform compositions, specified early on by the distinct Sec23/Sec24 heterodimer that forms the inner coat.

Results

Specific Sec23 Isoforms Are Required For Tip Growth

P. patens has seven *Sec23* genes, which group into four subclasses based on amino acid sequence similarity and gene structure (Fig1A). All seven *Sec23* genes are expressed in protonemal tissue (Fig1B). With the exception of *Sec23A*, at least one member of each subclass is highly expressed (Fig 1B). To determine if Sec23 plays a role in protonemal growth, we used transient RNA interference (RNAi) to silence the *Sec23* gene family. We selected regions of the coding sequences from *Sec23A*, *Sec23C*, *Sec23D* and *Sec23G* to silence each of the *Sec23* subclasses (Fig1A, solid lines under gene models). These sequence regions share a high degree of sequence similarity to the other gene in each subclass (Fig 1A,

148 dashed lines under gene models, Table S1) and would effectively simultaneously
149 silence both genes. By co-transforming the Sec23G RNAi construct together with
150 a construct containing the target sequences for *Sec23A*, *C* and *D*, we targeted the
151 entire *Sec23* gene family and discovered that silencing the seven *Sec23* genes
152 leads to a dramatic reduction in growth (Fig 1C and D). Surprisingly, we found
153 that silencing subclass III comprised of *Sec23D* and *Sec23E* resulted in a similarly
154 severe growth defect (Fig 1C and D). In contrast, silencing any of the other
155 subclasses did not affect growth (Fig 1C and D). These results demonstrated that
156 there is functional specificity among *Sec23* isoforms, with only subclass III
157 playing a critical role in protonemal growth, while the remaining five *Sec23*
158 isoforms appear to be dispensable.
159 To test whether *Sec23D* and *Sec23E* within subclass III are functionally
160 redundant, we designed RNAi constructs targeting the untranslated regions
161 (UTRs) of each gene (Fig 2A).Targeting the untranslated regions of both *Sec23D*
162 and *Sec23E* resulted in small unpolarized plants with an 85% reduction in plant
163 area as compared to control RNAi plants (Fig 2B and C). Silencing *Sec23D* alone
164 resulted in a 59% reduction in plant area, while silencing *Sec23E* did not affect
165 plant area (Fig 2B and C). Given that *Sec23D* is expressed seven times higher
166 than *Sec23E* (Fig 1B), it is possible that *Sec23D* contributes to protonemal growth
167 more than *Sec23E*. To test whether *Sec23E* can replace *Sec23D* function if
168 expressed at sufficient levels, we performed complementation studies by driving
169 the full-length coding sequence of *Sec23D* or *Sec23E* with the constitutive maize
170 ubiquitin promoter. Interestingly, the reduction in plant area resulting from
171 silencing of *Sec23D* was restored to similar levels when either *Sec23D* or *Sec23E*
172 full-length cDNAs were expressed (Fig 2B and C), indicating that *Sec23D* and
173 *Sec23E* are functionally redundant, and that the highly expressed *Sec23D* is the
174 predominant group III isoform critical for protonemal growth.
175
176 ***CRISPR-Cas9-mediated deletion of Sec23 isoforms***
177 Using transient RNAi, we were able to deduce that *Sec23* genes display
178 isoform specific functions during protonemal growth. However transient RNAi
179 assays are limited to phenotypic characterization of 7-day-old plants. To further
180 characterize the molecular functions of *Sec23*, we generated stable loss-of-

181 function mutants of *Sec23* genes using CRISPR-Cas9 mediated genome editing.
182 We targeted each gene with one protospacer located in the first coding exon (Fig
183 S1). We obtained single and higher-order mutants of *Sec23* genes carrying out-
184 of-frame mutations resulting in premature stop codons in their transcripts (Fig
185 S1A, Table S2). Consistent with the RNAi results, 7-day-old *Δsec23d* plants were
186 70% smaller than wild type plants while *Δsec23e* plants exhibited no growth
187 defects (Fig 3A and B). We isolated a number of *sec23d* null alleles (Fig S1A,
188 Table S2), which had similar growth phenotypes (Figure S1B). We also found
189 that in three-week-old plants regenerated from protoplasts, *Δsec23d-5* plants
190 were 62.6% smaller than wild type (Fig 3C and D), and Δ*sec23d-5* had fewer
191 gametophores compared to wild type (Fig 3C and E), suggesting that slow
192 growing protonemal tissues resulted in a developmental delay in the production
193 of gametophores.
194 Although it was possible to isolate many *Δsec23d-5* and *Δsec23e* single
195 mutants, we were unable to obtain *Δsec23de* double mutants either by targeting
196 *Sec23D* and *Sec23E* simultaneously or by targeting *Sec23D* in the *Δsec23e* single
197 mutant background. This suggests that deleting both *Sec23D* and *Sec23E* is
198 incompatible with protoplast regeneration, consistent with the severe growth
199 defects observed by simultaneously silencing *Sec23D* and *Sec23E* using RNAi.
200 Furthermore, we confirmed that none of the other *Sec23* genes were upregulated
201 in *Δsec23d-5* plants (Fig S1C), suggesting that the phenotypic consequences
202 observed were due specifically to loss of *Sec23D*.
203 Since the RNAi results suggested that all other *Sec23* subclasses were not
204 required for protonemal growth, we sought to isolate a stable line lacking
205 *Sec23A*, *Sec23B*, *Sec23C*, *Sec23F*, and *Sec23G* to determine if these genes
206 contribute to other aspects of plant growth and development. We successfully
207 isolated two independent quintuple mutant alleles *Δsec23abcfg-1* and
208 *Δsec23abcfg-2,* in which *Sec23A*, *Sec23B*, *Sec23C*, *Sec23F*, and *Sec23G* contained
209 lesions resulting in null alleles for each gene (Fig S3, Table S2). Most lesions were
210 small deletions or insertions. However, *Δsec23abcfg-1* contained a three
211 thousand base pair insertion in the *Sec23G* locus, still resulting in disruption of
212 the *Sec23G* locus (Fig S3, Table S2). We characterized both quintuple mutants
213 and found that while seven-day old *Δsec23abcfg-1* plants exhibited no detectable

214 growth defects, *Δsec23abcfg-2* plants exhibited a mild growth defect (Fig 3B and
215 C). However, three-week-old *Δsec23abcfg-1* plants were larger than wild type,
216 and *Δsec23abcfg-2* plants were indistinguishable from wild type (Fig 3D and E).
217 Interestingly, both *Δsec23abcfg-1* and *Δsec23abcfg-2* developed more
218 gametophores than wild type (Fig 3E), suggesting that these five *Sec23* genes
219 may negatively regulate gametophore development.
220 Even though the two quintuple mutant isolates, exhibited statistically
221 significant differences at different times in development between each other and
222 wild type, these were minor compared to the differences between wild type and
223 all isolated *Δsec23d* null mutants. To investigate whether the observed
224 differences might result from differential upregulation of *Sec23D* of *Sec23E* in the
225 *Δsec23abcfg* mutants thereby compensating for the loss of *Sec23ABCFG*
226 functions, we measured the expression levels of *Sec23D* and *Sec23E* transcripts
227 in *Δsec23abcfg-1, Δsec23abcfg-2*, and wild type. In 7-day-old plants, we found
228 that neither *Sec23D* nor *Sec23E* transcripts were elevated compared to
229 expression in wild type (Fig 3F), indicating that minor differences observed
230 between the two quintuple mutants were not readily explained by increased
231 expression of either *Sec23D* or *E*. Taken together, the phenotypic analyses of
232 stable *sec23* null plants suggest that *Sec23ABCF* and *G* do not contribute
233 substantially to establishment of juvenile moss tissues under laboratory growth
234 conditions. In contrast, *Sec23D* and *E* are essential.
235
236 ***Loss of Sec23D causes ER morphology defects and ER stress***
237 As a predicted member of the COPII complex, Sec23D likely mediates ER-
238 to-Golgi transport. However, it is unclear whether the *Δsec23d* growth defect is a
239 result of a general impairment of ER-to-Golgi transport, or the lack of specific
240 cargo sorted by Sec23D needed for protonemal growth. Studies in other
241 organisms have shown that blocking COPII function alters ER morphology
242 (Novick et al., 1980) and results in elevated levels of unfolded proteins in the ER,
243 leading to activation of the ER unfolded protein response (Belden, 2001; Chung
244 et al., 2016). To analyze Sec23D's function in ER-to-Golgi transport, we
245 investigated whether loss of Sec23D affects ER morphology and the ER unfolded
246 protein response. We used CRISPR-Cas9 mediated genome editing to knock out

247 Sec23D in a line where the ER is fluorescently labeled by targeting GFP to the ER
248 lumen (Fig S1, Table S2). When imaged with a confocal microscope, *Δsec23d-B11*
249 cells exhibited numerous ER dots (Fig 4A, red and cyan boxes), and 65% of
250 protonemal filaments contained large ER aggregates (Fig 4A, green and yellow
251 boxes), suggesting that loss of Sec23D causes abnormal accumulations of ER
252 domains, leading to severe ER morphology defect in *Δsec23d* cells.
253 If changes in ER morphology result from defective secretion at ER exit
254 sites, then proteins may be inadvertently accumulating in the ER, resulting in
255 upregulation of the unfolded protein response. To test this, we analyzed the
256 expression of an ER heat shock protein (Bip), which is a well-known ER stress
257 reporter in *Arabidopsis thaliana* (Noh et al., 2003; Srivastava et al., 2013;
258 Maruyama et al., 2014; Cho and Kanehara, 2017). *P. patens* has two *Bip* paralogs,
259 *Bip1* and *Bip2*. Since *Bip2* expression is low in protonemal tissue (Ortiz-Ramírez
260 et al., 2017), we tested whether *Bip1* is affected under conditions that induce ER
261 stress. Brefeldin A (BFA) inhibits protein secretion by disrupting ER-Golgi
262 integrity (Nebenfuhr, 2002; Niu et al., 2005). We found that after a 24-hour
263 treatment of BFA, expression of *Bip1* increased by about two-fold (Fig 4B),
264 indicating that *Bip1* is a plausible ER stress reporter in *P. patens*. Interestingly,
265 *Bip1* expression increased 5-fold in *Δsec23d* compared to in wild type (Fig 4C),
266 demonstrating that *Δsec23d* suffers from severe ER stress. In contrast,
267 *Δsec23abcfg-1*, which didn't exhibit significant growth defects, had normal levels
268 of *Bip1* expression (Fig 4C), and normal ER morphology (Fig 4A).
269
270 ***Disrupting Sec23D results in secretion defects to the Golgi apparatus and the***
271 ***plasma membrane***
272 ER morphology defects and elevated ER stress in *Δsec23d* suggest that
273 transport of secretory cargos might be blocked. We reasoned that proteins
274 destined to the Golgi and the plasma membrane would accumulate in the ER in
275 mutants with impaired ER to Golgi transport. To test this, we disrupted *Sec23D*
276 in lines that either express a YFP fusion of a Golgi resident protein (YFP-Golgi) or
277 an mCherry fusion of a plasma membrane protein (F-SNAP-mCherry) (Nelson et
278 al., 2007; Furt et al., 2012; van Gisbergen et al., 2018) (Fig S1, Table S2). Since it
279 would have been time-consuming to regenerate quintuple mutants in these two

280 backgrounds, we instead transformed the YFP-Golgi and F-SNAP-mCherry
281 markers into *Δsec23abcfg-1* plants. We selected lines that had similar expression
282 levels to control lines by measuring the total amount of fluorescence in cells.
283 In control YFP-Golgi lines, YFP signal accumulated in the Golgi with very
284 little fluorescence observed in the rest of the cell (Fig 5A). In contrast in *Δsec23d-*
285 *S2*, while YFP fluorescence still accumulated in the Golgi, a large portion of the
286 fluorescent signal that was presumably retained in the ER was observed
287 diffusely throughout the cell (Fig 5A). To quantify Golgi secretion efficiency, we
288 calculated the fluorescence intensity ratio of the signal in the Golgi divided by the
289 signal in the cell. A high ratio value indicates efficient secretion, as observed in
290 the control lines (Fig 5B). In contrast, *Δsec23d-S2* exhibited a significantly lower
291 fluorescence intensity ratio (Fig 5B), indicating that loss of Sec23D impairs
292 secretion to the Golgi. Imaging of *Δsec23abcfg-1* YFP-Golgi and its control line
293 revealed that the majority of the YFP signal localizes to the Golgi with the Golgi
294 to cytoplasm ratios in *Δsec23abcfg*-1 indistinguishable from the control (Fig 5B),
295 suggesting that secretion to the Golgi is not affected in the quintuple mutant.
296 Many proteins transported in COPII-coated vesicles ultimately reside at the
297 plasma membrane. In wild type cells, the fluorescent marker F-SNAP-mCherry
298 accumulated on the plasma membrane, with only a very small amount of
299 fluorescence detected inside the cell (Fig 5C). In *Δsec23d,* a large portion of the
300 mCherry signal was retained in the cell, labeling the ER network (Fig 5C). To
301 quantify secretion efficiency to the plasma membrane, we calculated the
302 fluorescence intensity ratio of the plasma membrane to the intensity within the
303 cell. We found that the ratio in *Δsec23d* was significantly lower than that of its
304 control line (Fig 5D), indicating that loss of Sec23D inhibits secretion of plasma
305 membrane bound proteins.
306 Interestingly, we found that the F-SNAP-mCherry signal was also retained
307 inside the cell in the *Δsec23abcfg-1* mutant, readily observing labeling of the ER
308 network (Fig 5C). In addition, the fluorescence intensity ratio in *Δsec23abcfg-1*
309 was lower in comparison to the ratio in its control line (Fig 5D). However, the
310 ratio in *Δsec23abcfg-1* was still significantly higher than the ratio in *Δsec23d*,
311 suggesting that secretion of plasma membrane proteins is impaired in
312 *Δsec23abcfg-1* but to a lower extent than in *Δsec23d*. These data together with

313 the lack of a growth defect in protonomata in the *Δsec23abcfg-1* mutant suggest
314 that Sec23A, B, C, F, and G contribute to protein secretion particularly to the
315 plasma membrane, but importantly their cargos are not essential for polarized
316 growth in protonemata.
317
318 ***Sec23D localizes to discrete puncta associated with the ER***
319 If Sec23 is a bona fide COPII component, then we would expect that Sec23
320 isoforms should associate with the ER. To test this, we inserted sequences in the
321 genome of a line expressing GFP in the ER lumen encoding for three tandem
322 mRuby2 (hereafter, mRuby2) in frame with the coding sequences of the three
323 mostly highly expressed protonematal *Sec23* genes: *Sec23B*, *Sec23D* and *Sec23G*
324 (Fig 1B, Fig S3A, B). To ensure that tagging *Sec23D* did not affect its function, we
325 measured plant area from 7-day old regenerated protoplasts and found that
326 *Sec23D-mRuby2* grew indistinguishably from the control lines (Fig S3C),
327 suggesting that Sec23D-mRuby2 is functional. By analogy, we reasoned that
328 tagging *Sec23B* and *G* would also be functional. To ensure we did not observe any
329 possible dominant negative impacts as a result of the tagging, we performed
330 growth assays of 7-day old plants regenerated from protoplasts and observed
331 that *Sec23B-mRuby2* was indistinguishable from the control and *Sec23G-mRuby2*
332 was slightly smaller (Fig. S3C).
333 Imaging with confocal microscopy revealed that Sec23D, Sec23B and
334 Sec23G localized to punctate structures (Fig 6A). Interestingly, Sec23G-mRuby2
335 puncta were larger than the punctate structures found in Sec23D- and Sec23B-
336 mRuby2 lines (Fig 6A and C), suggesting that Sec23G compartments maybe
337 different from Sec23B and D. While Sec23 isoforms labeled structures of
338 different sizes, all three proteins labeled puncta that were proximal to the ER
339 (Fig 6A). Co-localization measurements using Pearson's Correlation Coefficient
340 suggested that Sec23D, B and G puncta positively correlated with the ER. To
341 ensure that this correlation was significant, we flipped the ER image both
342 vertically and horizontally and repeated the correlation analysis and found that
343 the correlation coefficients were significantly lower (Fig 6B).
344

345 ***Sec24 isoforms differentially contribute to protonemal growth***

346 Sec23 forms an obligate heterodimer with Sec24 to build the inner coat of
347 COPII. We reasoned that if a specific Sec24 isoform dimerizes with Sec23D, then
348 loss of that Sec24 isoform should result in a phenotype similar to that observed
349 for *Δsec23d*. *P. patens* has seven *Sec24* genes, which is the same number of genes
350 found in the *Sec23* gene family. Similar to *Sec23*, there are four subclasses of
351 *Sec24* genes and six of the seven *Sec24* genes exist in closely related pairs (Fig
352 7A). We found that *Sec24E* was not expressed in 8-day old protonemal tissue,
353 while the other six *Sec24* genes were expressed (Fig 7B). Of these six genes,
354 *Sec24D* exhibited the lowest expression while the other five Sec24 genes were
355 expressed at similar levels (Fig 7A). Taking advantage of the high sequence
356 similarity within each *Sec24* subclass, regions of the coding sequences from
357 *Sec24B*, *Sec24C*, and *Sec24F* were cloned to generate RNAi constructs (Table S1)
358 that would target both members of the subclass (Fig 7A). Interestingly, silencing
359 *Sec24C* and *Sec24D* resulted in severe growth defects, with a 79% reduction in
360 plant area (Fig 7C and D). Silencing *Sec24F* and *Sec24G* also impaired growth, but
361 to a lesser extent resulting in a 48% reduction in plant area (Fig 7C and D). On
362 the other hand, silencing *Sec24A* and *Sec24B* did not affect growth, although both
363 genes were expressed at high levels. These data suggest that similar to Sec23,
364 there is isoform specificity among *Sec24* genes. Due to the similar RNAi
365 phenotypes observed for Sec23D/E and Sec24C/D, we hypothesized that
366 Sec23D/E and Sec24C/D form heterodimers.

367 To test for direct interaction between Sec23D and Sec24 isoforms, we
368 conducted a yeast two-hybrid assay using Sec23D as bait and Sec24B, Sec24C,
369 Sec24D, and Sec24F as preys. Full-length cDNAs of these genes were isolated
370 from protonemal tissue, and with the exception of *Sec24C*, only one transcript
371 was identified from each locus. For *Sec24C*, we isolated two alternative
372 transcripts: Sec24C V3.1 and Sec24C V3.3. Sec24C V3.1 is truncated at the N
373 terminus compared to Sec24C V3.3, lacking the first exon and the first half of the
374 second exon (Fig S4). Pairwise yeast two-hybrid assays demonstrated that
375 Sec23D strongly interacts with both versions of Sec24C and with Sec24D. We
376 observed a weaker interaction between Sec23D and Sec24B, but no detectable
377 interaction between Sec23D and Sec24F (Fig7E).

378 If Sec24C/D heterodimerizes with Sec23D, then we would expect
379 Sec24C/D localization pattern to be similar to Sec23D. To test this, we inserted
380 mEGFP (Vidali et al., 2009) in frame with the C-terminus of Sec24C at its
381 endogenous locus. We found that Sec24C-mEGFP localized to punctate structures
382 (Fig 7F) similar to Sec23D-mRuby (Fig 6A). While we attempted to tag both
383 Sec23D and Sec24C with a fluorescent protein in the same line, we were unable
384 to isolate these lines, suggesting that Sec23/Sec24 heterodimerization may be
385 impaired when both proteins are tagged. To test if Sec24C localization depends
386 on functional Sec23D, we used CRISPR-Cas9 mediated genome editing to disrupt
387 *Sec23D* in the Sec24C-mEGFP line (Fig S1, Table S2). We discovered that when
388 *Sec23D* was disrupted, Sec24C-mEGFP no longer localized to puncta and was
389 diffuse throughout the cytoplasm (Fig 7F), indicating that Sec24C localization
390 depends on Sec23D.
391
392 **Discussion**
393 The large number of genes encoding components of COPII in plants
394 together with functional studies in Arabidopsis (De Craene et al., 2014; Chung et
395 al., 2016; Barlow and Dacks, 2018; Brandizzi, 2018)(Faso et al., 2009; Qu et al.,
396 2017; Tanaka et al., 2013) have led to the hypothesis that gene expansion
397 underlies increased functional diversification required for complex secretory
398 processes that pattern and build plant cells. Evidence suggests that functional
399 diversification could stem from tissue/developmental specific expression (Hino
400 et al., 2011; Lee et al.; Hanton et al., 2009) or from the formation of COPII
401 complexes comprised of unique isoform compositions (Zeng et al., 2015).
402 However, it remains unclear whether unique COPII complexes mediate transport
403 of specific cargos or accumulate at some ER exit sites and not at others. Here, by
404 analyzing the role of Sec23 isoforms in protonemal development, we have
405 provided evidence for formation of distinct ER exit sites and the requirement of
406 only Sec23D/E for transport of cargos uniquely required for tip growth.
407 In particular, we discovered that one of the Sec23 pairs, Sec23D/E, plays
408 an essential role in protonemal growth. Several lines of evidence suggest that
409 Sec23D functions as a bona fide COPII component. First, *Δsec23d* plants had
410 abnormal ER morphology and elevated ER stress consistent with a block in cargo

411 secretion from the ER. Second, secretion to both the Golgi and the plasma
412 membrane was inhibited. Third, Sec23D localized to puncta near the ER. Due to
413 differential expression levels, we found that Sec23D is more important for
414 protonemal growth than Sec23E. However, when expressed at sufficient levels,
415 Sec23E can rescue loss of Sec23D indicating that Sec23D and E are functionally
416 redundant. The inability to recover a double mutant lacking both Sec23D and E
417 suggests that together these two genes are essential for moss viability. Given that
418 viability in moss is measured in the ability to generate protonemata, which is a
419 tip-growing tissue, we reason that Sec23D and E are essential for tip growth. In
420 support of this, *Δsec23d* protonemal cells grow significantly slower than wild
421 type leading to smaller plants that develop gametophores late. However, once
422 gametophores form they are morphologically normal, suggesting that Sec23D
423 function is specifically required during tip growth.
424 Using RNAi and stable knockouts, we found that the remaining five Sec23
425 genes were dispensable for formation of both protonemata and gametophores.
426 One possible explanation for this finding is that Sec23A, B, C, F and G have
427 functionally diversified no longer playing a role in ER to Golgi transport.
428 However, our data suggest otherwise. In protonemata, we observed secretion
429 defects of plasma membrane cargo in *Δsec23abcfg* plants. Given that *Sec23B, F,*
430 and *G* are expressed at similar levels to *Sec23D* in protonemata and Sec23B and G
431 localize proximal to the ER, it is likely that Sec23B, F and G contribute to COPII
432 function in protonemata. However, in contrast to Sec23D, their cargos may not
433 be essential for tip growth. Furthermore, if COPII function is required for
434 secretion underlying gametophore formation, we would have expected to
435 observe a mutant combination leading to defective gametophore formation. Yet,
436 we found that both *Δsec23d* and *Δsec23abcfg* formed morphologically normal
437 gametophores, suggesting that Sec23D and Sec23A, B, C, F and G are functionally
438 redundant for COPII-mediated secretion required to shape gametophores. If, on
439 the other hand, COPII is not required for gametophore formation, then future
440 experiments conditionally removing Sec23D/E in *Δsec23abcfg* plants would be
441 expected to form normal gametophores and would be an excellent tool to
442 identify COPII-independent secretion pathways in plants, which are thought to

443 play a role in transport of tonoplast resident proteins such as the vacuolar H+-
444 ATPase, VHA-a3 (Viotti et al., 2013).
445 While Sec23B and G formed puncta associated with the ER, these puncta
446 were different from each other and Sec23D. Sec23G formed large dots near the
447 ER, whereas Sec23D and B were much smaller. Formation of larger domains
448 suggests that Sec23G may be involved in the secretion of larger cargo from the
449 ER and provides evidence that moss has morphologically distinct ER exit sites.
450 Given that Sec23D contributes to both Golgi and plasma membrane
451 secretion, while Sec23A, B, C, F and G contribute to plasma membrane secretion,
452 it is plausible to suggest that tip growth requires intact Golgi secretion. In
453 *Δsec23d* plants cargos essential for tip growth are either inefficiently carried
454 from the ER to the Golgi or are not properly processed in the Golgi due to severe
455 reductions in secretion to the Golgi. Perhaps there is a larger burden for
456 carbohydrates synthesized by enzymes in the Golgi to generate a tip growing cell
457 wall as compared to a diffusely growing cell wall. To test this, future studies will
458 focus on identifying cargos that have been differentially affected in *Δsec23d*
459 versus *Δsec23abcfg* plants. Comparative mass spectrometry of isolated
460 microsomes and plasma membrane extracts in these mutant backgrounds could
461 be very informative. In addition, quantitatively measuring secretion of known
462 Golgi resident carbohydrate biosynthetic enzymes and plasma membrane
463 complexes such as cellulose and callose synthases in these mutants could help to
464 narrow down cargo specificity.
465 As a COPII component, Sec23D should form a heterodimer with at least
466 one of the seven *P. patens* Sec24 isoforms. Directed two hybrid assays
467 demonstrated that Sec23D interacted most strongly with Sec24C and Sec24D.
468 Furthermore, plants lacking the *Sec24C/D* gene pair phenocopied *Sec23D/E* RNAi
469 plants. We also found that Sec24C localizes to puncta throughout the cytoplasm
470 and this localization depends on Sec23D. Taken together these data suggest that
471 Sec23D and Sec24C, the most highly expressed gene in the *Sec24C/D* pair,
472 heterodimerize. Due to the strong and unique phenotype associated with loss of
473 Sec23D/Sec24C, we hypothesize that Sec23D together with its partner Sec24C,
474 carry cargo required specifically for tip growth. The findings that Sec23D
475 preferentially binds to Sec24C/D and their loss of function results in the same

476 defects in tip growth are consistent with studies in *Arabidopsis* showing that
477 Sar1A and Sec23A form a unique interaction mediating functional specificity
478 (Zeng et al., 2015).
479 Taking advantage of the facile molecular genetic manipulation and
480 imaging in moss protonemal development, our study has shown that the
481 expanded *Sec23* gene family in moss is multi-faceted. We found evidence that the
482 *Sec23* gene family exhibits aspects of functional redundancy, differential gene
483 expression, as well as isoform specificity for COPII complex formation, ER exit
484 site formation, and importantly transport of essential cargos required for tip
485 growth. Building upon the tools developed in this study, future studies will be
486 able to characterize the remaining COPII components, thereby providing a
487 complete picture of how gene expansions in COPII have been deployed in the
488 evolution of this organism.
489
490 **Materials and Methods**
491 ***Expression analyses***
492 To quantify expression of the *Sec23* and *Sec24* genes family members
493 (Table S3), as well as *Bip1* (Pp3c10_17310), we isolated total RNA from 8-day old
494 plants (various genotypes, as needed for the particular experiment) regenerated
495 from protoplasts using the RNeasy Plant mini prep kit (Qiagen). cDNA was
496 prepared from 1μg of total RNA using SuperScriptIII reverse transcriptase kit,
497 following the manufacturer's recommendation (Invitrogen). qPCR assays were
498 conducted with Luna Universal qPCR Master Mix (New England Biolabs).
499 Primers for qRT-PCR analyses are listed in Table S4. After confirming that
500 amplification efficiencies (calculated from standard curves) were similar for
501 each set of primers (Table S4), relative expression levels were calculated, and
502 expression of Ubiquitin 10 was used for normalization. All experiments had
503 three technical replicates and three biological replicates.
504
505 ***Constructs***
506 The Sec23 and Sec24 RNAi constructs were generated by PCR
507 amplification of either the coding sequence or 5' and 3' untranslated region
508 (UTR) of *Sec23* or *Sec24* from *P. patens* cDNA using primers indicated in Table S4.

509 PCR fragments were cloned into pENTR-D-TOPO (Invitrogen) following the
510 manufacturer's recommendations and the resulting vectors were sequenced. The
511 Sec23ACD-RNAi and Sec23 UTR-RNAi constructs were generated by stitching
512 together multiple PCR fragments and then directionally cloned into pENTR-D-
513 TOPO as previously described (Vidali et al., 2007). LR clonase (Invitrogen)
514 reactions were used to transfer either the coding sequence or 5' and 3' UTR
515 sequences the RNAi vector pUGGi (Bezanilla et al., 2005) generating the Sec23
516 UTRi or Sec24-CDSi constructs, respectively. Restriction enzyme digestion was
517 used to verify these constructs.
518 Expression constructs were generated by PCR amplifying *Sec23D* and
519 *Sec23E* coding sequences from *P. patens* cDNA using a 5' CACC sequence on the
520 specific primers for oriented cloning into the pENTR-D-TOPO vector
521 (Invitrogen). LR clonase (Invitrogen) reactions were used to transfer these
522 coding sequence into pTH-Ubi-Gate vectors (Vidali et al., 2007).
523 *Sec23* and *Sec24* tagging constructs were generated by PCR amplifying
524 genomic sequences upstream and downstream of the stop codon for *Sec23D*,
525 *Sec23B*, *Sec23G* and *Sec24C* using the primers in Table S4. For *Sec23D* and *Sec24C*,
526 we used homologous recombination. The distance between the 5' and 3'
527 homology arms was 500bp for both *Sec23D* and *Sec24C*, which when inserted
528 correctly the tagging construct replaces these 500bp with sequences encoding
529 for the fluorescent protein and an antibiotic resistance cassette (Fig S3). Using
530 BP clonase (Invitrogen), homology arms were transferred to vectors, generating
531 homology arm entry clones. Four-fragment recombination reactions were used
532 to assemble the homology arms, fluorescent protein sequence, and the antibiotic
533 resistance cassette into pGEM-gate (Vidali et al., 2009). For *Sec23B* and *Sec23G*
534 tagging, we used CRISPR Cas9-mediated homology directed repair. 5' and 3'
535 homology arms upstream and downstream of the stop codon, with a distance
536 between these two arms of 38bp for *Sec23B* and 131bp for *Sec23G* were PCR
537 amplified from genomic DNA. Using BP clonase (Invitrogen), homology arms
538 were transferred to vectors, generating homology arm entry clones, as described
539 recently (Mallett et al., 2019). Three-fragment recombination reactions were
540 used to assemble the homology arms and the fluorescent protein sequence into
541 pGEM-gate. We chose the CRISPR-Cas9 protospacer close to the stop codon.

542 Protospacers for CRISPR-Cas9 mediated mutagenesis and HDR were
543 designed with the CRISPOR online software (crispor.tefor.net) (Haeussler et al.,
544 2016). Protospacers were selected with high specificity scores and low off-target
545 frequency. Specific overhangs sequences were added to facilitate downstream
546 cloning. Protospacers were synthesized as oligonucleotides (Table S4) and
547 annealed as described (Mallett et al., 2019). Annealed protospacer fragments
548 were transferred to vectors using Instant Sticky-End Ligation Master Mix (New
549 England Biolabs). *Sec23B* and *G* protospacers designed to tag these genes via
550 HDR as well as *Sec23A*, *D* and *E* protospacers designed to knock out these genes
551 were ligated into pENTR-PpU6-sgRNA-L1L2 (Mallett et al., 2019). *Sec23B* and *F*
552 protospacers designed to knock out these genes were ligated into pENTR-PpU6-
553 sgRNA-L1L5 (Mallett et al., 2019). Sec23C and G protospacers designed to knock
554 out these genes were ligated into pENTR-PpU6-sgRNA-R5L2 (Mallett et al.,
555 2019). LR clonase (Invitrogen) was used to assemble the protospacer containing
556 vectors into pZeo-Cas9-Gate, pMH-Cas9-Gate, or pMK-Cas9-Gate vectors (Mallett
557 et al., 2019), as needed. Two-fragment recombination reactions were used to
558 assembly dual targeting mutagenesis vectors for *Sec23B* and *C*, and for *Sec23F*
559 and *G*. Restriction enzyme digestion and sequencing was used to verify these
560 constructs.
561 *Sec23D*, *Sec24B*, *CV3.1*, *CV3.3*, *D* and *F* coding sequences were amplified
562 from *P. patens* cDNA using a 5' CACC sequence on the specific primers for
563 oriented cloning into pENTR-D-TOPO (Invitrogen). LR clonase (Invitrogen)
564 reactions were used to transfer these coding sequences into yeast 2-hybrid
565 vectors. *Sec23D* was transferred to pGBKT7-Gate (Bascom Jr et al., 2018), and all
566 Sec24 genes were transferred to pGADT7-Gate (Bascom Jr et al., 2018).
567
568 ***Tissue propagation, transformation, and genotyping***
569 All moss lines were propagated weekly by moderate homogenization in
570 water and pipetting onto a permeable cellophane covered solid media, as
571 described previously (Wu and Bezanilla, 2014). Tissue was grown at room
572 temperature in Percival growth chambers, under 85 $\mu mol_{photons}/m^2s$ light with
573 long-day conditions. PEG-mediated transformations were performed as
574 previously described to generate stable lines (Wu and Bezanilla, 2014), CRISPR-

575 Cas9 genome edited lines (Mallett et al., 2019) and perform transient RNAi
576 (Vidali et al., 2007).
577 To genotype mutants generated by CRISPR-Cas9 mutagenesis, we
578 extracted DNA from plants that were 3-4 weeks old (0.5-1cm in diameter) using
579 the protocol described in (Augustine et al., 2011). For editing experiments, we
580 used primers (Table S4) surrounding the expected Cas9 cleavage site (~300-400
581 bp on each side). T7 endonuclease assay was used to screen candidate mutants
582 as described (Mallett et al., 2019). For homology-directed repair tagging and
583 homologous recombination tagging, we used primers (Table S4) outside of the
584 homology region to avoid amplification of residual DNA donor template.
585
586 ***Imaging and morphometric analysis of growth assays***
587 For transient RNAi, complementation analyses, and growth assays of
588 stable lines, plants regenerated from protoplasts were photographed seven days
589 after protoplasting. For transient RNAi and complementation analyses plants
590 lacking nuclear GFP signal were imaged because these are the plants that are
591 actively silencing as described previously (Bezanilla et al., 2005; Vidali et al.,
592 2007). For growth assays of stable lines any regenerated plant was imaged.
593 Images were acquired with a 1X objective using a stereomicroscope (Leica
594 MZ16FA or Nikon SMZ25) equipped with a CCD camera (Leica DF300FX or
595 Nikon digital sight DS-Fi2). Chlorophyll fluorescence and any nuclear GFP signal
596 were acquired simultaneously using filters (480/40, dichroic 505 (Leica) or
597 dichroic 510 (Nikon), emission 510 long pass). Exposure settings were
598 maintained constant throughout an experiment. 3-week old plants regenerated
599 from protoplasts were imaged with white light on a Nikon SMZ25
600 stereomicroscope equipped with a Nikon digital sight DS-Fi2 color camera.
601 To quantify plant area, individual plants were cropped from images and
602 the red channel, representing chlorophyll fluorescence of the plant, was
603 separated from the RGB image. Threshold settings were set manually for all
604 plants within an experiment. To quantify brightfield images of 3-week-old plants,
605 the blue channel, representing chlorophyll fluorescence of the plant, was
606 separated from the RGB image and thresholded. Total area was calculated from
607 the largest thresholded object in the selected window. All images analysis was

608 done using macros (Galotto et al., 2019) written for ImageJ. Analysis of variation
609 (ANOVA) for multiple comparisons was performed with Kaleidagraph (Synergy)
610 using the Tukey HSD post hoc tests. The alpha for statistical significance was set
611 to 0.05.
612
613 ***Laser scanning confocal microscope imaging and quantification***
614 For imaging Sec23D localization and dynamics, 5 to 8-day old plants
615 regenerated from protoplasts were placed onto an agar pad in Hoagland's buffer
616 (4mM KNO_3, 2mM KH_2PO_4, 1mM $Ca(NO_3)_2$, 89μM Fe citrate, 300μM $MgSO_4$,
617 9.93μM H_3BO_3, 220nM $CuSO_4$, 1.966μM $MnCl_2$, 231nM $CoCl_2$, 191nM ZnSO4,
618 169nM KI, 103nM Na_2MoO_4, and 1% sucrose), covered by a glass cover slip and
619 sealed with VALAP (1:1:1 parts of Vaseline, lanoline, and paraffin). For imaging
620 ER morphology, Golgi resident protein secretion, F-SNAP-mCherry secretion, we
621 used microfluidic imaging chambers (Bascom et al., 2016). Ground protonemal
622 tissue was gently pipetted into the central part of the device followed by an
623 infusion of Hoagland's medium. Then the chamber was submerged Hoagland's
624 medium, and placed under constant 85 $\mu mol_{photons}/m^2s$ light.
625 Images were acquired on a Nikon A1R confocal microscope system with a
626 1.4 NA 60X oil immersion objective (Nikon) at room temperature. Image
627 acquisition was controlled by NIS-Element AR 4.1 software (Nikon). All images
628 were processed using Image J software with background subtraction, enhanced
629 contrast and smoothing. All settings were the standard Image J settings.
630 For quantification of secretion to the Golgi, confocal Z-stacks of individual
631 cells were converted to a maximum intensity projection. YFP fluorescence
632 intensity with the same expression pattern was normalize into the same range in
633 ImageJ. Using thresholding it was possible to isolate the fluorescence intensity of
634 Golgi dot (Golgi intensity) and the fluorescence intensity of rest of the cell
635 (background intensity). These values were used to calculate the ratio of Golgi
636 intensity to background intensity. For quantification of secretion to the plasma
637 membrane, the medial focal plane was selected for analysis. The mCherry
638 fluorescence intensity was normalize into the same range using ImageJ. Using
639 thresholding it was possible to isolate the fluorescence intensity of the plasma
640 membrane (PM) and the fluorescence intensity of rest of the cell (internal).

641 These values were used to calculate the ratio of Golgi intensity to background
642 intensity. To quantify the Pearson's Correlation Coefficient, we analyzed single
643 focal planes with the Coloc2 plugin in Fiji comparing the original images as well
644 as horizontally and vertically flipped ER-GFP images. To quantify the size of
645 Sec23B, D and G puncta, we thresholded single focal plane images to isolate the
646 dots and then followed with particle analysis in Fiji. Dots resulting from the
647 merge of two or more puncta were removed from the analysis. For all data,
648 analysis of variation (ANOVA) for multiple comparisons was performed with
649 Kaleidagraph (Synergy) using the Tukey HSD post hoc tests. The alpha for
650 statistical significance was set to 0.05.
651
652 ***2-Hybrid Assays***
653 pGBKT7-Sec23D was transformed into Y2H Gold competent cells (Takara-
654 Bio) and pGADT7-Sec24 constructs were transformed into Y187 competent cells
655 (Takara-Bio). Y2H Gold cells and Y187 cells were mated and then diploids were
656 selected. Diploids were tested for 2-hybrid interactions with serial dilutions of
657 overnight cultures with the same optical density value equal amount using
658 minimal medium lacking Tryptophan (selects for pGBKT7 plasmid), Leucine
659 (selects for pGADT7 plasmid), Histidine and Adenine (promoters driving
660 expression of genes essential for the synthesis of these amino acids are activated
661 when there is a positive 2-hybrid interaction).
662
663 **Author contributions**
664 M.C. and M.B. designed the research. M.C., S.W., and J.E.O. performed the
665 research. M.C., S.W. and M.B. wrote the article.
666
667 **Acknowledgements**
668 We thank members of the Bezanilla lab for careful reading of the
669 manuscript. M.C. received support from the Plant Biology Graduate Program at
670 the University of Massachusetts, Amherst. This work was supported by
671 Dartmouth College and grants from the National Science Foundation (MCB-
672 1330171 and MCB-1715785 to M.B.).
673

674 **References**

675 **Aridor, M.** (2018). COPII gets in shape: Lessons derived from morphological
676 aspects of early secretion. Traffic **19**: 823–839.
677
678 **Aridor, M., Fish, K.N., Bannykh, S., Weissman, J., Roberts, T.H., Lippincott-**
679 **Schwartz, J., and Balch, W.E.** (2001). The Sar1 Gtpase Coordinates
680 Biosynthetic Cargo Selection with Endoplasmic Reticulum Export Site
681 Assembly. Journal of Cell Biology **152**: 213–230.
682
683 **Aridor, M., Weissman, J., Bannykh, S., Nuoffer, C., and Balch, W.E.** (1998).
684 Cargo Selection by the COPII Budding Machinery during Export from the
685 ER. Journal of Cell Biology **141**: 61–70.
686
687 **Augustine, R.C., Pattavina, K.A., Tüzel, E., Vidali, L., and Bezanilla, M.** (2011).
688 Actin interacting protein1 and actin depolymerizing factor drive rapid
689 actin dynamics in Physcomitrella patens. Plant Cell **23**: 3696–3710.
690
691 **Barlow, L.D. and Dacks, J.B.** (2018). Seeing the endomembrane system for the
692 trees: Evolutionary analysis highlights the importance of plants as models
693 for eukaryotic membrane-trafficking. Seminars in Cell & Developmental
694 Biology **80**: 142–152.
695
696 **Barlowe, C.** (2003). Signals for COPII-dependent export from the ER: what's the
697 ticket out? Trends in Cell Biology **13**: 295–300.
698
699 **Barlowe, C. and Helenius, A.** (2016). Cargo Capture and Bulk Flow in the Early
700 Secretory Pathway. Annu. Rev. Cell Dev. Biol. **32**: 197–222.
701
702 **Barlowe, C. and Schekman, R.** (1993). SEC12 encodes a guanine-nucleotide-
703 exchange factor essential for transport vesicle budding from the ER.
704 Nature **365**: 347–349.
705
706 **Bascom, C.S., Wu, S.-Z., Nelson, K., Oakey, J., and Bezanilla, M.** (2016). Long-
707 Term Growth of Moss in Microfluidic Devices Enables Subcellular Studies
708 in Development. Plant Physiology **172**: 28–37.
709
710 **Bascom Jr, C., Burkart, G.M., Mallett, D.R., O'Sullivan, J.E., Tomaszewski, A.J.,**
711 **Walsh, K., and Bezanilla, M.** (2018). Systematic survey of the function of
712 ROP regulators and effectors during tip growth in the moss
713 Physcomitrella patens. J. Exp. Bot. **70**: 447–457.
714
715 **Belden, W.J.** (2001). Role of Erv29p in Collecting Soluble Secretory Proteins into
716 ER-Derived Transport Vesicles. Science **294**: 1528–1531.
717
718 **Bezanilla, M., Perroud, P.-F., Pan, A., Klueh, P., and Quatrano, R.S.** (2005). An
719 RNAi system in Physcomitrella patens with an internal marker for
720 silencing allows for rapid identification of loss of function phenotypes.
721 Plant Biol (Stuttg) **7**: 251–257.
722

723 **Bi, X., Corpina, R.A., and Goldberg, J.** (2002). Structure of the Sec23/24–Sar1
724 pre-budding complex of the COPII vesicle coat. Nature **419**: 271–277.
725
726 **Brandizzi, F.** (2018). Transport from the endoplasmic reticulum to the Golgi in
727 plants: Where are we now? Seminars in Cell & Developmental Biology **80**:
728 94–105.
729
730 **Brandizzi, F. and Barlowe, C.** (2013). Organization of the ER–Golgi interface for
731 membrane traffic control. Nat Rev Mol Cell Biol **14**: 382–392.
732
733 **Cho, Y. and Kanehara, K.** (2017). Endoplasmic Reticulum Stress Response in
734 Arabidopsis Roots. Front. Plant Sci. **8**.
735
736 **Chung, K.P., Zeng, Y., and Jiang, L.** (2016). COPII Paralogs in Plants: Functional
737 Redundancy or Diversity? Trends in Plant Science **21**: 758–769.
738
739 **De Craene, J.-O., Courte, F., Rinaldi, B., Fitterer, C., Herranz, M.C., Schmitt-**
740 **Keichinger, C., Ritzenthaler, C., and Friant, S.** (2014). Study of the Plant
741 COPII Vesicle Coat Subunits by Functional Complementation of Yeast
742 Saccharomyces cerevisiae Mutants. PLoS ONE **9**: e90072.
743
744 **Faso, C., Chen, Y.-N., Tamura, K., Held, M., Zemelis, S., Marti, L., Saravanan,**
745 **R., Hummel, E., Kung, L., Miller, E., Hawes, C., and Brandizzi, F.** (2009).
746 A Missense Mutation in the Arabidopsis COPII Coat Protein Sec24A
747 Induces the Formation of Clusters of the Endoplasmic Reticulum and
748 Golgi Apparatus. The Plant Cell **21**: 3655–3671.
749
750 **Fath, S., Mancias, J.D., Bi, X., and Goldberg, J.** (2007). Structure and
751 Organization of Coat Proteins in the COPII Cage. Cell **129**: 1325–1336.
752
753 **Furt, F., Lemoi, K., Tüzel, E., and Vidali, L.** (2012). Quantitative analysis of
754 organelle distribution and dynamics in Physcomitrella patens protonemal
755 cells. BMC Plant Biol. **12**: 70.
756
757 **Galotto, G., Bibeau, J.P., and Vidali, L.** (2019). Automated Image Acquisition
758 and Morphological Analysis of Cell Growth Mutants in Physcomitrella
759 patens. In Plant Cell Morphogenesis, F. Cvrčková and V. Žárský, eds,
760 Methods in Molecular Biology. (Springer New York: New York, NY), pp.
761 307–322.
762
763 **Giraudo, C.G. and Maccioni, H.J.F.** (2003). Endoplasmic Reticulum Export of
764 Glycosyltransferases Depends on Interaction of a Cytoplasmic Dibasic
765 Motif with Sar1. MBoC **14**: 3753–3766.
766
767 **van Gisbergen, P.A.C., Wu, S.-Z., Chang, M., Pattavina, K.A., Bartlett, M.E., and**
768 **Bezanilla, M.** (2018). An ancient Sec10-formin fusion provides insights
769 into actin-mediated regulation of exocytosis. J. Cell Biol. **217**: 945–957.
770

771 **Haeussler, M., Schönig, K., Eckert, H., Eschstruth, A., Mianné, J., Renaud, J.-B.,**
772 **Schneider-Maunoury, S., Shkumatava, A., Teboul, L., Kent, J., Joly, J.-S.,**
773 **and Concordet, J.-P.** (2016). Evaluation of off-target and on-target
774 scoring algorithms and integration into the guide RNA selection tool
775 CRISPOR. Genome Biol. **17**: 148.
776
777 **Hanna, M.G., Peotter, J.L., Frankel, E.B., and Audhya, A.** (2018). Membrane
778 Transport at an Organelle Interface in the Early Secretory Pathway: Take
779 Your Coat Off and Stay a While: Evolution of the metazoan early secretory
780 pathway. BioEssays **40**: 1800004.
781
782 **Hanton, S.L., Matheson, L.A., Chatre, L., and Brandizzi, F.** (2009). Dynamic
783 organization of COPII coat proteins at endoplasmic reticulum export sites
784 in plant cells. The Plant Journal **57**: 963–974.
785
786 **Hino, T., Tanaka, Y., Kawamukai, M., Nishimura, K., Mano, S., and Nakagawa,**
787 **T.** (2011). Two Sec13p Homologs, AtSec13A and AtSec13B, Redundantly
788 Contribute to the Formation of COPII Transport Vesicles in *Arabidopsis*
789 *thaliana*. Bioscience, Biotechnology, and Biochemistry **75**: 1848–1852.
790
791 **Jensen, D. and Schekman, R.** (2011). COPII-mediated vesicle formation at a
792 glance. Journal of Cell Science **124**: 1–4.
793
794 **Khoriaty, R. et al.** (2018). Functions of the COPII gene paralogs SEC23A and
795 SEC23B are interchangeable in vivo. Proc Natl Acad Sci USA **115**: E7748–
796 E7757.
797
798 **Lee, M.H., Lee, S.H., Kim, H., Jin, J.B., Kim, D.H., and Hwang, I.** A WD40 Repeat
799 Protein, Arabidopsis Sec13 Homolog 1, May Play a Role in Vacuolar
800 Trafficking by Controlling the Membrane Association of AtDRP2A.: 10.
801
802 **Mallett, D.R., Chang, M., Cheng, X., and Bezanilla, M.** (2019). Efficient and
803 modular CRISPR-Cas9 vector system for Physcomitrella patens. Plant
804 Direct **3**: e00168-15.
805
806 **Mancias, J.D. and Goldberg, J.** (2007). The Transport Signal on Sec22 for
807 Packaging into COPII-Coated Vesicles Is a Conformational Epitope.
808 Molecular Cell **26**: 403–414.
809
810 **Maruyama, D., Sugiyama, T., Endo, T., and Nishikawa, S.** (2014). Multiple BiP
811 Genes of Arabidopsis thaliana are Required for Male Gametogenesis and
812 Pollen Competitiveness. Plant and Cell Physiology **55**: 801–810.
813
814 **Mossessova, E., Bickford, L.C., and Goldberg, J.** (2003). SNARE selectivity of
815 the COPII coat. Cell **114**: 483–495.
816
817 **Nakano, A. and Muramatsu, M.** (1989). A Novel GTP-binding Protein, Sarlp, Is
818 Involved in Transport from the Endoplasmic Reticulum to the Golgi
819 Apparatus. The Journal of Cell Biology **109**: 2677–2691.

Nakano, R.T., Matsushima, R., Ueda, H., Tamura, K., Shimada, T., Li, L., Hayashi, Y., Kondo, M., Nishimura, M., and Hara-Nishimura, I. (2009). GNOM-LIKE1/ERMO1 and SEC24a/ERMO2 Are Required for Maintenance of Endoplasmic Reticulum Morphology in Arabidopsis thaliana. The Plant Cell **21**: 3672–3685.

Nebenfuhr, A. (2002). Brefeldin A: Deciphering an Enigmatic Inhibitor of Secretion. Plant physiology **130**: 1102–1108.

Nelson, B.K., Cai, X., and Nebenführ, A. (2007). A multicolored set of in vivo organelle markers for co-localization studies in Arabidopsis and other plants. Plant J. **51**: 1126–1136.

Niu, T.-K., Pfeifer, A.C., Lippincott-Schwartz, J., and Jackson, C.L. (2005). Dynamics of GBF1, a Brefeldin A-Sensitive Arf1 Exchange Factor at the Golgi□V. Molecular Biology of the Cell **16**: 1213–1222.

Noh, S.-J., Kwon, C.S., Oh, D.-H., Moon, J.S., and Chung, W.-I. (2003). Expression of an evolutionarily distinct novel BiP gene during the unfolded protein response in Arabidopsis thaliana. Gene **311**: 81–91.

Novick, P., Field, C., and Schekman, R. (1980). Identification of 23 complementation groups required for post-translational events in the yeast secretory pathway. Cell **21**: 205–215.

Nufer, O. (2003). ER export of ERGIC-53 is controlled by cooperation of targeting determinants in all three of its domains. Journal of Cell Science **116**: 4429–4440.

Ortiz-Ramírez, C., Michard, E., Simon, A.A., Damineli, D.S.C., Hernandez-Coronado, M., Becker, J.D., and Feijó, J.A. (2017). GLUTAMATE RECEPTOR-LIKE channels are essential for chemotaxis and reproduction in mosses. Nature **549**: 91–95.

Qu, X., Zhang, R., Zhang, M., Diao, M., Xue, Y., and Huang, S. (2017). Organizational innovation of apical actin filaments drives rapid pollen tube growth and turning. Mol Plant **10**: 930–947.

Rensing, S.A., Goffinet, B., Meyberg, R., Wu, S.-Z., and Bezanilla, M. (2020). The Moss *Physcomitrium* (*Physcomitrella*) *patens* : A Model Organism for Non-Seed Plants. Plant Cell **32**: 1361–1376.

Salama, N.R., Yeung, T., and Schekman, R.W. The Secl3p complex and reconstitution of vesicle budding from the ER with purified cytosolic proteins. The EMBO Journal **12**: 4073–4082.

867 **Srivastava, R., Deng, Y., Shah, S., Rao, A.G., and Howell, S.H.** (2013). BINDING
868 PROTEIN Is a Master Regulator of the Endoplasmic Reticulum Stress
869 Sensor/Transducer bZIP28 in *Arabidopsis*. Plant Cell **25**: 1416–1429.
870
871 **Stagg, S.M., Gürkan, C., Fowler, D.M., LaPointe, P., Foss, T.R., Potter, C.S.,**
872 **Carragher, B., and Balch, W.E.** (2006). Structure of the Sec13/31 COPII
873 coat cage. Nature **439**: 234–238.
874
875 **Stagg, S.M., LaPointe, P., Razvi, A., Gürkan, C., Potter, C.S., Carragher, B., and**
876 **Balch, W.E.** (2008). Structural Basis for Cargo Regulation of COPII Coat
877 Assembly. Cell **134**: 474–484.
878
879 **Takagi, J., Renna, L., Takahashi, H., Koumoto, Y., Tamura, K., Stefano, G.,**
880 **Fukao, Y., Kondo, M., Nishimura, M., Shimada, T., Brandizzi, F., and**
881 **Hara-Nishimura, I.** (2013). MAIGO5 Functions in Protein Export from
882 Golgi-Associated Endoplasmic Reticulum Exit Sites in Arabidopsis. The
883 Plant Cell **25**: 4658–4675.
884
885 **Tanaka, Y., Nishimura, K., Kawamukai, M., Oshima, A., and Nakagawa, T.**
886 (2013). Redundant function of two Arabidopsis COPII components,
887 AtSec24B and AtSec24C, is essential for male and female gametogenesis.
888 Planta **238**: 561–575.
889
890 **Vidali, L., Augustine, R.C., Kleinman, K.P., and Bezanilla, M.** (2007). Profilin is
891 essential for tip growth in the moss Physcomitrella patens. Plant Cell **19**:
892 3705–3722.
893
894 **Vidali, L., van Gisbergen, P.A.C., Guérin, C., Franco, P., Li, M., Burkart, G.M.,**
895 **Augustine, R.C., Blanchoin, L., and Bezanilla, M.** (2009). Rapid formin-
896 mediated actin-filament elongation is essential for polarized plant cell
897 growth. Proc. Natl. Acad. Sci. U.S.A. **106**: 13341–13346.
898
899 **Viotti, C. et al.** (2013). The Endoplasmic Reticulum Is the Main Membrane
900 Source for Biogenesis of the Lytic Vacuole in *Arabidopsis*. Plant Cell **25**:
901 3434–3449.
902
903 **Whittle, J.R.R. and Schwartz, T.U.** (2010). Structure of the Sec13–Sec16 edge
904 element, a template for assembly of the COPII vesicle coat. The Journal of
905 Cell Biology **190**: 347–361.
906
907 **Wu, S.-Z. and Bezanilla, M.** (2014). Myosin VIII associates with microtubule
908 ends and together with actin plays a role in guiding plant cell division.
909 eLife Sciences **3**: e03498.
910
911 **Zeng, Y., Chung, K.P., Li, B., Lai, C.M., Lam, S.K., Wang, X., Cui, Y., Gao, C., Luo,**
912 **M., Wong, K.-B., Schekman, R., and Jiang, L.** (2015). Unique COPII
913 component AtSar1a/AtSec23a pair is required for the distinct function of
914 protein ER export in *Arabidopsis thaliana*. Proc Natl Acad Sci USA **112**:
915 14360–14365.

916
917
918 **Figure Legends**

919 **Figure 1. *Sec23D* and *E* are required for polarized growth.** (A) Gene models
920 of the *P. patens Sec23* genes are shown with exons indicated by boxes and
921 introns by thin black lines. Coding and untranslated regions are denoted by thick
922 and thin boxes, respectively. The lines underneath the gene models represent
923 sequence regions targeted by Sec23 RNAi constructs. Scale bar is 500bp. (B)
924 Relative expression of *Sec23* genes normalized to UBIQUITIN10 in 8-day-old
925 wild-type moss plants regenerated from protoplasts. N = 3, Error bars are s.e.m.
926 (C) Representative chlorophyll autofluorescence images of 7-day-old plants
927 regenerated from protoplasts expressing the indicated RNAi constructs. Scale
928 bar, 100 μm. (D) Quantification of plant area is based on the area of the
929 chlorophyll autofluorescence and is presented normalized to the area of the
930 control. Means are indicated by horizontal lines. Letters indicate groups with
931 significantly different means as determined by a one-way ANOVA with a Tukey
932 *post hoc* test (α=0.05).
933

934 **Figure 2. *Sec23D* and *Sec23E* are functionally redundant.** (A) *Sec23D* and
935 *Sec23E* gene models are shown with exons indicated by boxes and introns by
936 thin black lines. Coding and untranslated regions are denoted by thick and thin
937 boxes, respectively. The lines underneath the gene models represent sequence
938 regions that were targeted by Sec23D or Sec23E UTR RNAi constructs. Scale bar
939 is 500bp. (B) Representative chlorophyll autofluorescence images of 7-day-old
940 plants regenerated from protoplasts expressing the indicated constructs. Scale
941 bar, 100 μm. (C) Quantification of plant area was normalized to the control.
942 Letters indicate groups with significantly different means as determined by a
943 one-way ANOVA with a Tukey *post hoc* test (α=0.05).
944

945 **Figure 3. CRISPR-Cas9-mediated deletion of *Sec23* isoforms demonstrates**
946 **that *Sec23D* is critical for protonemal growth.** (A) Representative chlorophyll
947 autofluorescence images of 7-day old plants with the indicated genotype
948 regenerated from protoplasts. Scale bar, 100μm. (B) Quantification of plant area

949 normalized to the wild type control. (C) Representative 3-week old moss plants
950 with the indicated genotype. Scale bar, 1mm. (D) Quantification of the plant area
951 of 3-week old moss plants normalized to that of the wild type control. (E)
952 Number of gametophores in 3-week old moss plants. Letters in (B, D-E) indicate
953 groups with significantly different means as determined by a one-way ANOVA
954 with a Tukey *post hoc* test (α=0.05). (F) Relative expression of *Sec23D* and *E*
955 genes normalized to UBIQUITIN10 in 8-day-old wild type and *Δsec23abcfg-1*, and
956 *Δsec23abcfg-2* moss plants regenerated from protoplasts. N=3, Error bars are
957 s.e.m. No significant difference was determined by a one-way ANOVA with a
958 Tukey *post hoc* test (α=0.05).
959
960 **Figure 4. Loss of Sec23D causes ER morphology defects and ER stress.** (A)
961 Laser scanning confocal images of the ER labeled with GFP-KDEL in the indicated
962 genotype. Colored boxes highlight large and small ER aggregates found in the
963 *Δsec23d-B11* mutant. Scale bar 10 μm. (B, C) Relative expression of *PpBip1* in 8-
964 day old moss plants regenerated from protoplasts. N=3, p<0.01. Error bars are
965 s.e.m. In (B) BFA-treated plants were normalized to DMSO-treated plants and in
966 (C) null mutants were normalized to wild type plants.
967
968 **Figure 5. Deletion of *Sec23D* results in secretion defects to the Golgi**
969 **apparatus and the plasma membrane.** (A) Representative maximum
970 projections of confocal images of the indicated genotypes expressing a YFP-Golgi
971 marker. Scale bar, 10 μm. (B) Quantification of the fluorescence intensity ratio
972 within the Golgi to the background. (C) Representative medial sections of
973 confocal images of the indicated genotypes expressing a plasma membrane
974 marker (FSnap-mCherry). Scale bar, 10 μm. Letters in (B, D) indicate groups with
975 significantly different means as determined by a one-way ANOVA with a Tukey
976 *post hoc* test (α=0.05).
977
978 **Figure 6. Sec23 isoforms localize to structures with distinct sizes.** (A)
979 Representative medial sections of confocal images of lines where the indicated
980 Sec23 gene was endogenously tagged with mRuby in a line that expresses GFP in
981 the ER. (B) Pearson's correlation coefficient measured between the Sec23

982 labeled lines and ER-GFP. O, original ER image; V, vertically flipped ER image; H,
983 horizontally flipped ER image. Letters indicate groups with significantly different
984 means as determined by a one-way ANOVA with a Tukey *post hoc* test (α=0.05)
985 (C) Quantification of average dot size in the Sec23 images. Asterisks denote
986 p<0.001 as determined by a one-way ANOVA with a Tukey *post hoc* test (α=0.05).
987
988 **Figure 7. *Sec24* isoforms differentially contribute to protonemal growth.**
989 (A) *Sec24* gene models are shown with exons indicated by boxes and introns by
990 thin black lines. Coding and untranslated regions are denoted by thick and thin
991 boxes, respectively. Lines underneath the models represent sequence regions
992 that were targeted by Sec24 RNAi constructs. Scale bar, 1000 bp. (B) Relative
993 expression of *Sec24* genes normalized to UBIQUITIN10 in 8-day-old wild-type
994 moss plants regenerated from protoplasts. N=3, Error bars are s.e.m. (C)
995 Representative chlorophyll autofluorescence images of 7-day old plants
996 regenerated from protoplasts expressing the indicated RNAi constructs. Scale
997 bar, 100 μm. (D) Quantification of plant area is based on the area of the
998 chlorophyll autofluorescence and is presented normalized to the area of the
999 control. Means are indicated by horizontal lines. Letters indicate groups with
1000 significantly different means as determined by a one-way ANOVA with a Tukey
1001 *post hoc* test (α=0.05). (E) Serial dilutions of yeast strains carrying 2-hybrid
1002 vectors testing for interaction between Sec23D and the indicated Sec24 isoforms.
1003 Growth indicates that tested proteins interact. *Sec24C* V3.1 and V3.3 are two
1004 splice variants isolated from 7-day old protonemal tissue. Positive control:
1005 murine p53 insert and SV40 large T-antigen; Negative control: human lamin and
1006 SV40 large T-antigen (Clontech). (F) Representative maximum projections of
1007 confocal images of endogenously tagged Sec24C-mEGFP in the indicated
1008 genotypes. Large globular structures are chloroplasts, which autofluoresce under
1009 these imaging conditions. Scale bar, 5 μm.

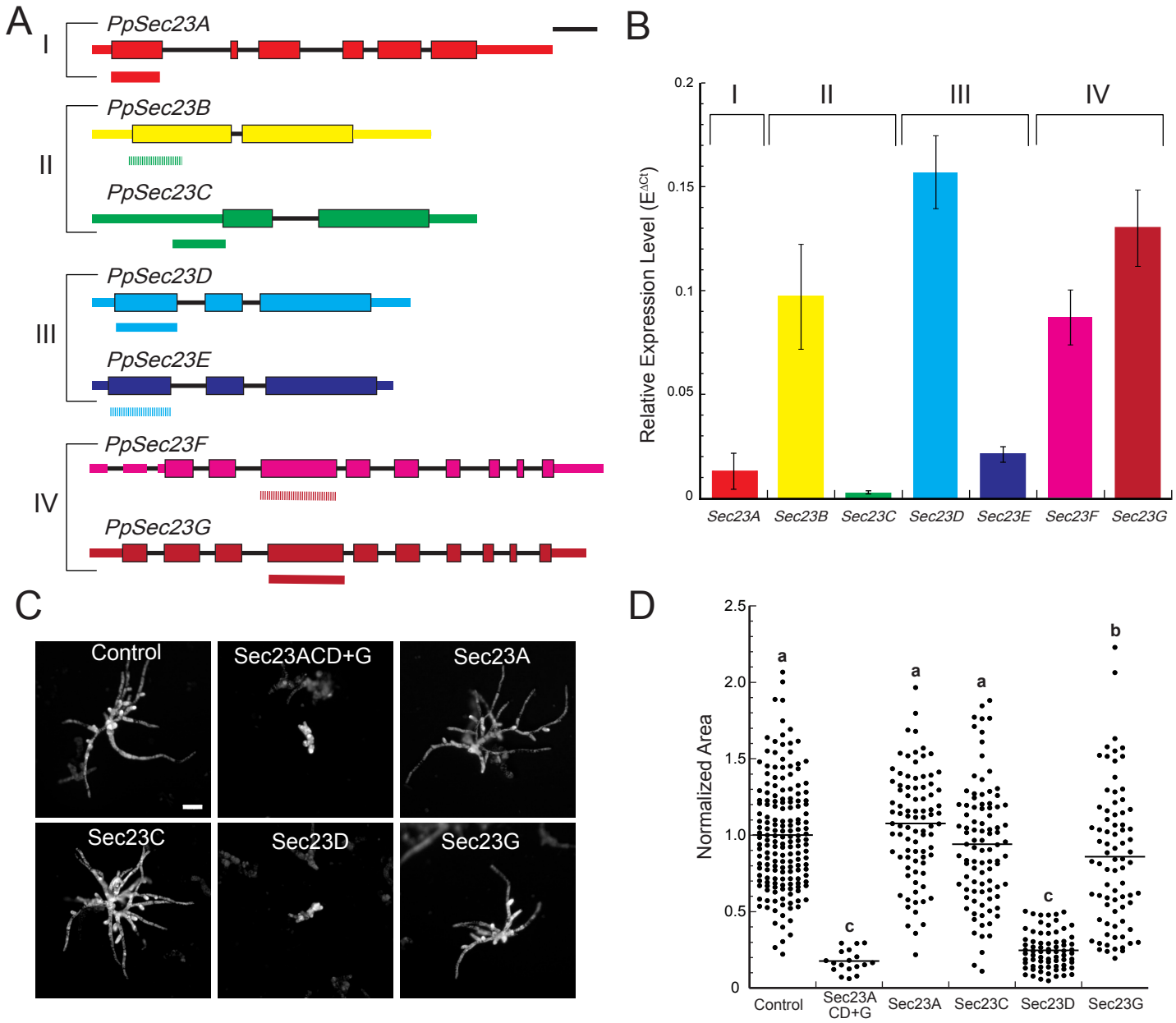

Figure 1. *Sec23D* and *E* are required for polarized growth. (A) Gene models of the *P. patens Sec23* genes are shown with exons indicated by boxes and introns by thin black lines. Coding and untranslated regions are denoted by thick and thin boxes, respectively. The lines underneath the gene models represent sequence regions targeted by Sec23 RNAi constructs. Scale bar is 500bp. (B) Relative expression of *Sec23* genes normalized to UBIQUITIN10 in 8-day-old wild-type moss plants regenerated from protoplasts. N = 3, Error bars are s.e.m. (C) Representative chlorophyll autofluorescence images of 7-day-old plants regenerated from protoplasts expressing the indicated RNAi constructs. Scale bar, 100 µm. (D) Quantification of plant area is based on the area of the chlorophyll autofluorescence and is presented normalized to the area of the control. Means are indicated by horizontal lines. Letters indicate groups with significantly different means as determined by a one-way ANOVA with a Tukey *post hoc* test (α=0.05).

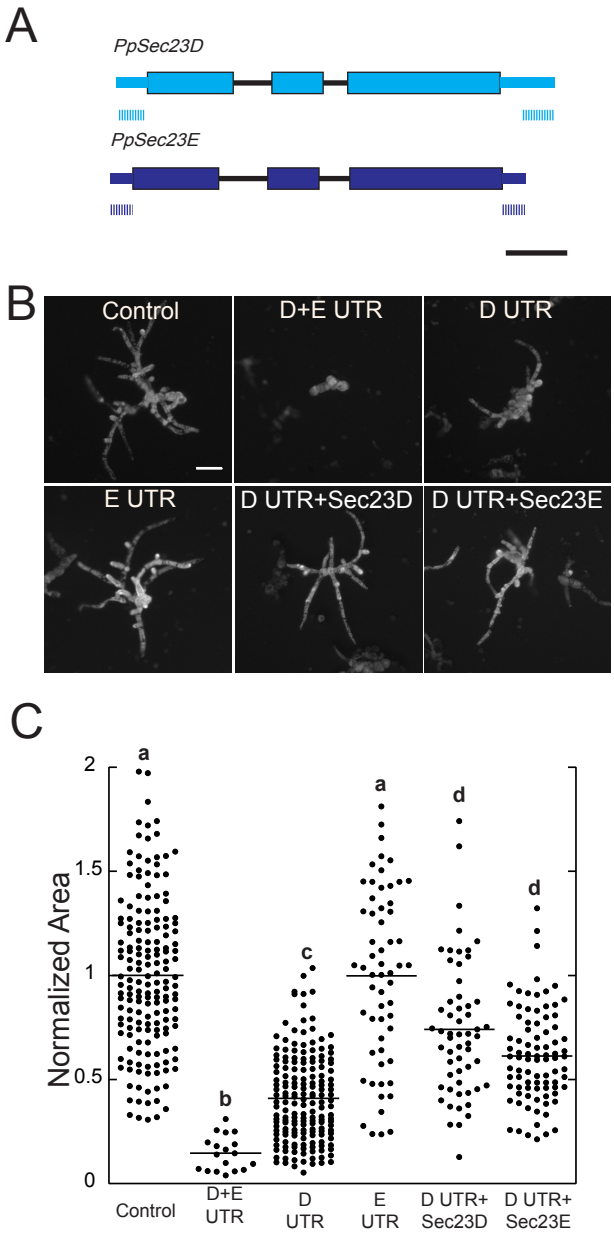

Figure 2. *Sec23D* and *Sec23E* are functionally redundant. (A) *Sec23D* and *Sec23E* gene models are shown with exons indicated by boxes and introns by thin black lines. Coding and untranslated regions are denoted by thick and thin boxes, respectively. The lines underneath the gene models represent sequence regions that were targeted by Sec23D or Sec23E UTR RNAi constructs. Scale bar is 500bp. (B) Representative chlorophyll autofluorescence images of 7-day-old plants regenerated from protoplasts expressing the indicated constructs. Scale bar, 100 µm. (C) Quantification of plant area was normalized to the control. Letters indicate groups with significantly different means as determined by a one-way ANOVA with a Tukey *post hoc* test (α=0.05).

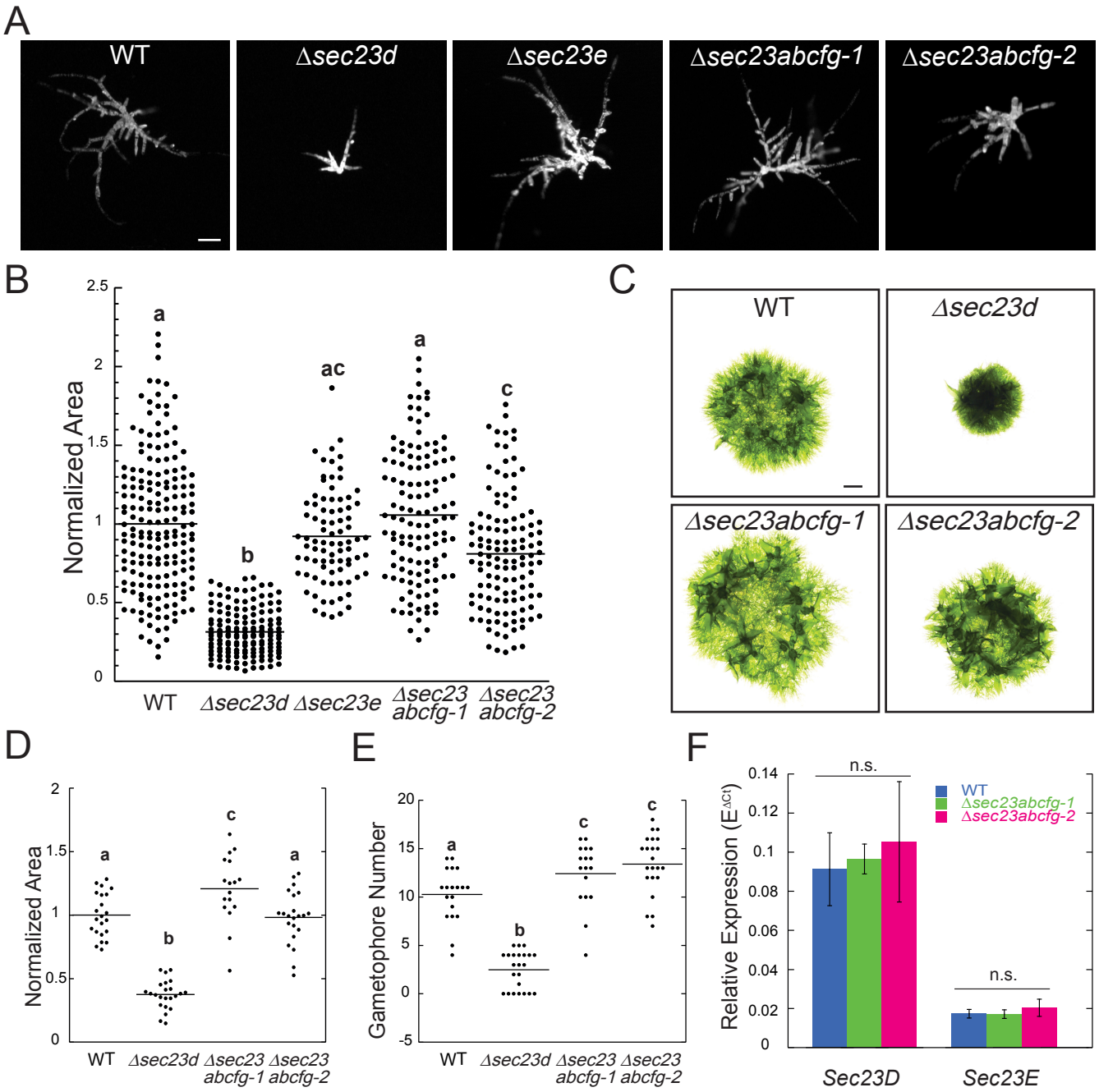

Figure 3. CRISPR-Cas9-mediated deletion of *Sec23* isoforms demonstrates that *Sec23D* is critical for protonemal growth. (A) Representative chlorophyll autofluorescence images of 7-day old plants with the indicated genotype regenerated from protoplasts. Scale bar, 100µm. (B) Quantification of plant area normalized to the wild type control. (C) Representative 3-week old moss plants with the indicated genotype. Scale bar, 1mm. (D) Quantification of the plant area of 3-week old moss plants normalized to that of the wild type control. (E) Number of gametophores in 3-week old moss plants. Letters in (B, D-E) indicate groups with significantly different means as determined by a one-way ANOVA with a Tukey *post hoc* test (α=0.05). (F) Relative expression of *Sec23D* and *E* genes normalized to UBIQUITIN10 in 8-day-old wild type and Δ*sec23abcfg-1*, and Δ*sec23abcfg-2* moss plants regenerated from protoplasts. N=3, Error bars are s.e.m. No significant difference was determined by a one-way ANOVA with a Tukey *post hoc* test (α=0.05).

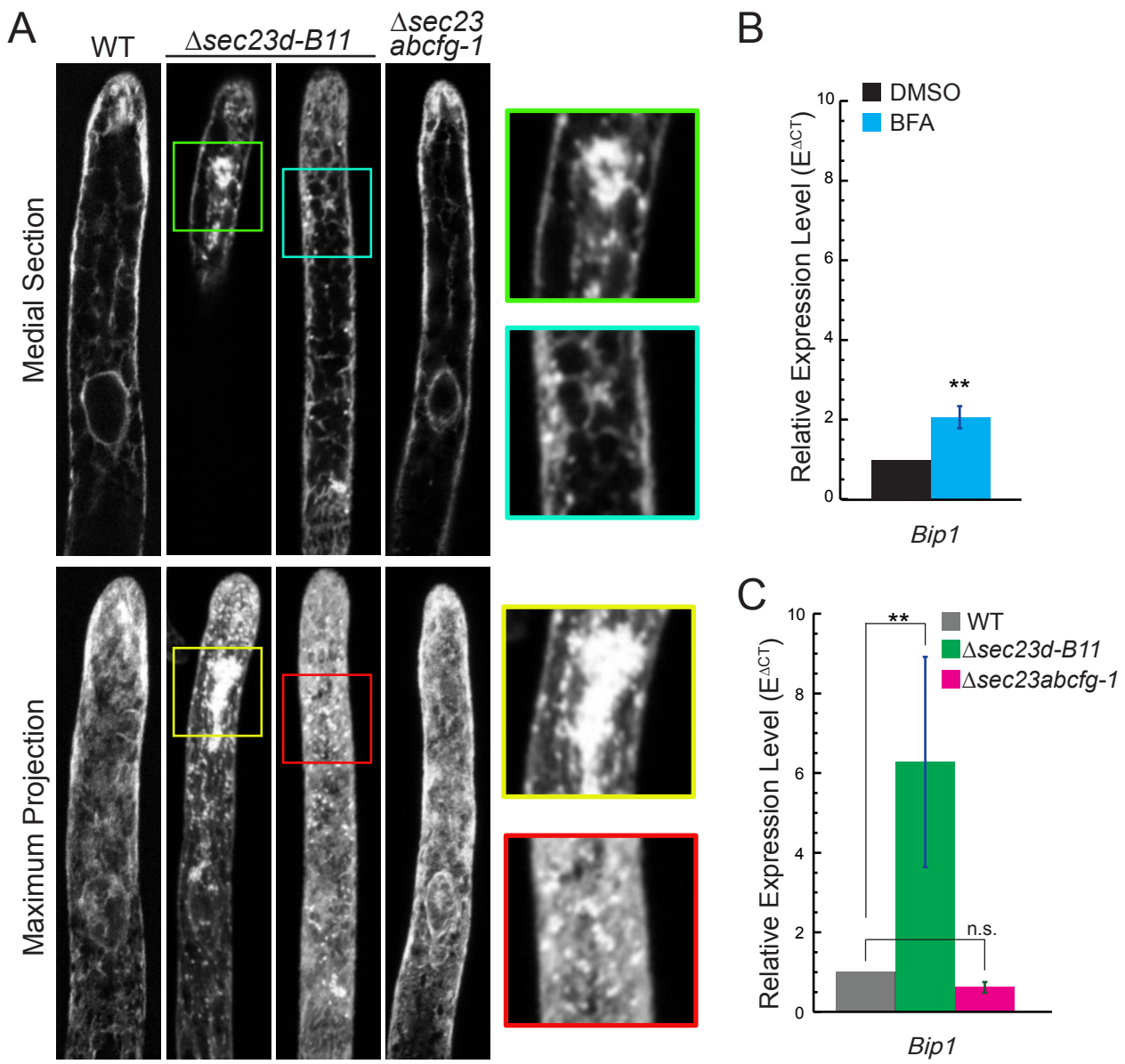

Figure 4. Loss of Sec23D causes ER morphology defects and ER stress. (A) Laser scanning confocal images of the ER labeled with GFP-KDEL in the indicated genotype. Colored boxes highlight large and small ER aggregates found in the Δ*sec23d-B11* mutant. Scale bar 10 µm. (B, C) Relative expression of *PpBip1* in 8-day old moss plants regenerated from protoplasts. N=3, $p<0.01$. Error bars are s.e.m. In (B) BFA-treated plants were normalized to DMSO-treated plants and in (C) null mutants were normalized to wild type plants.

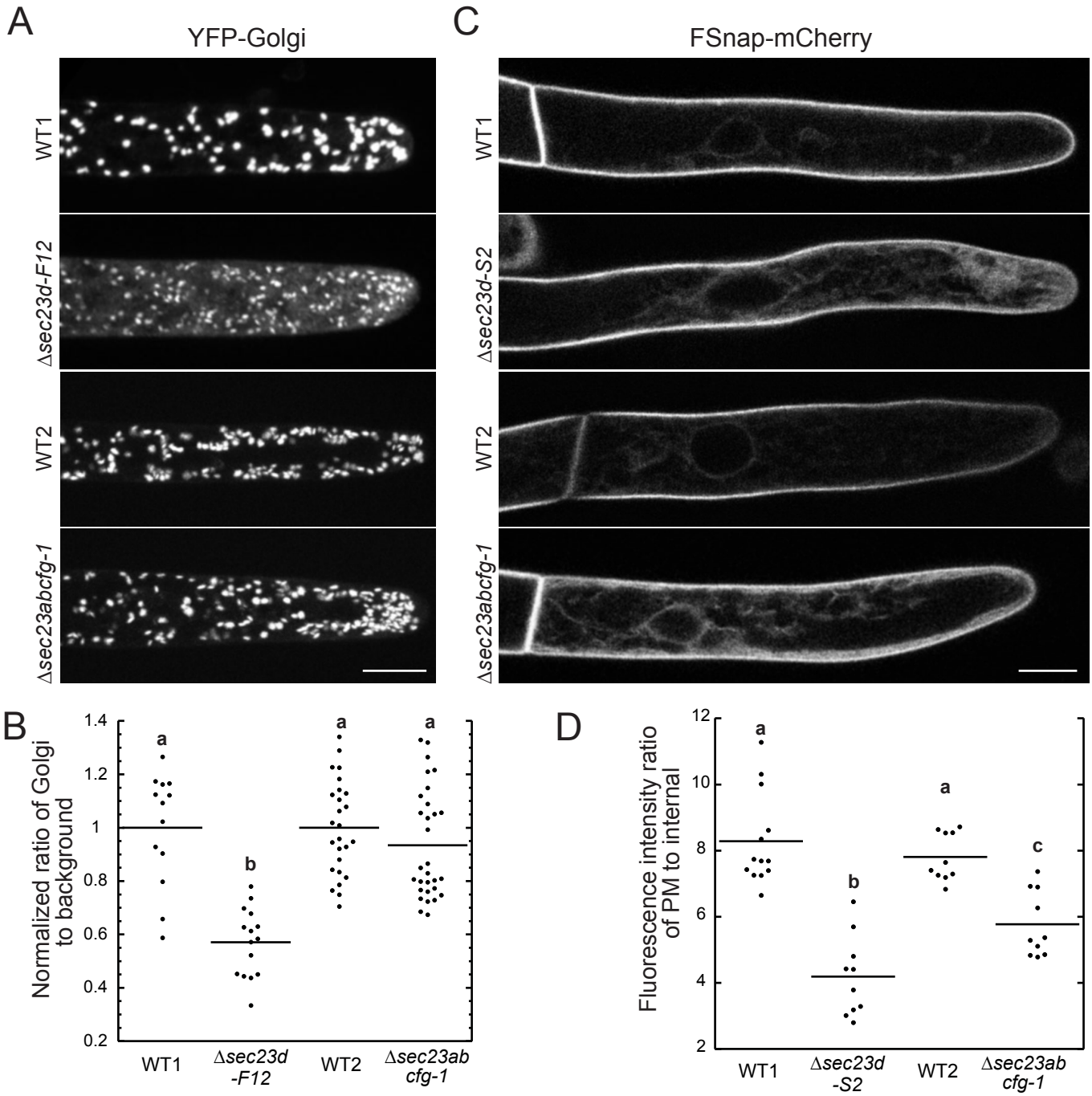

Figure 5. Deletion of *Sec23D* results in secretion defects to the Golgi apparatus and the plasma membrane. (A) Representative maximum projections of confocal images of the indicated genotypes expressing a YFP-Golgi marker. Scale bar, 10 μm. (B) Quantification of the fluorescence intensity ratio within the Golgi to the background. (C) Representative medial sections of confocal images of the indicated genotypes expressing a plasma membrane marker (FSnap-mCherry). Scale bar, 10 μm. Letters in (B, D) indicate groups with significantly different means as determined by a one-way ANOVA with a Tukey *post hoc* test (α=0.05).

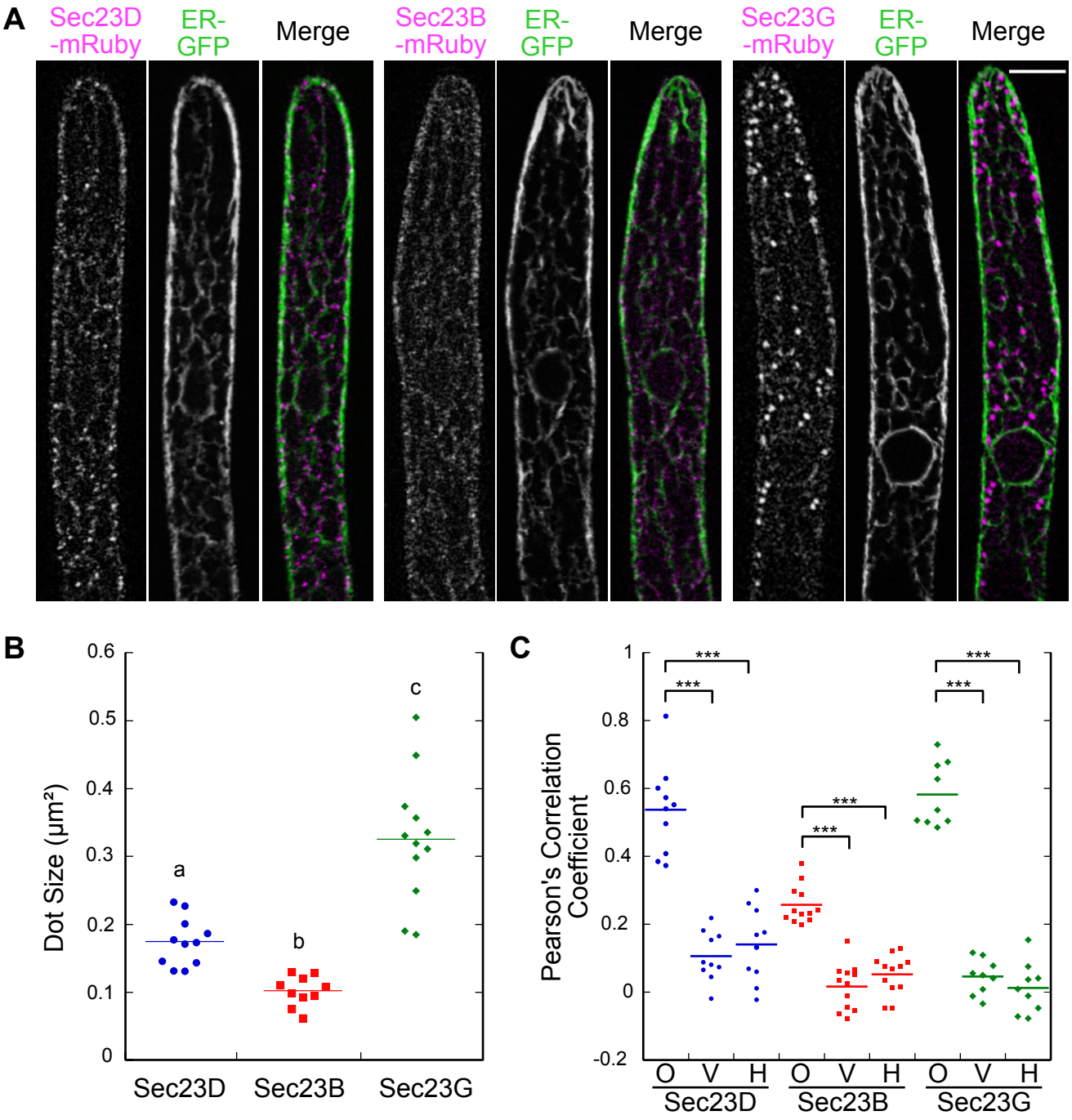

Figure 6. Sec23 isoforms localize to structures with distinct sizes. (A) Representative medial sections of confocal images of lines where the indicated Sec23 gene was endogenously tagged with mRuby in a line that expresses GFP in the ER. (B) Pearson's correlation coefficient measured between the Sec23 labeled lines and ER-GFP. O, original ER image; V, vertically flipped ER image; H, horizontally flipped ER image. Letters indicate groups with significantly different means as determined by a one-way ANOVA with a Tukey *post hoc* test (α=0.05) (C) Quantification of average dot size in the Sec23 images. Asterisks denote p<0.001 as determined by a one-way ANOVA with a Tukey *post hoc* test (α=0.05).

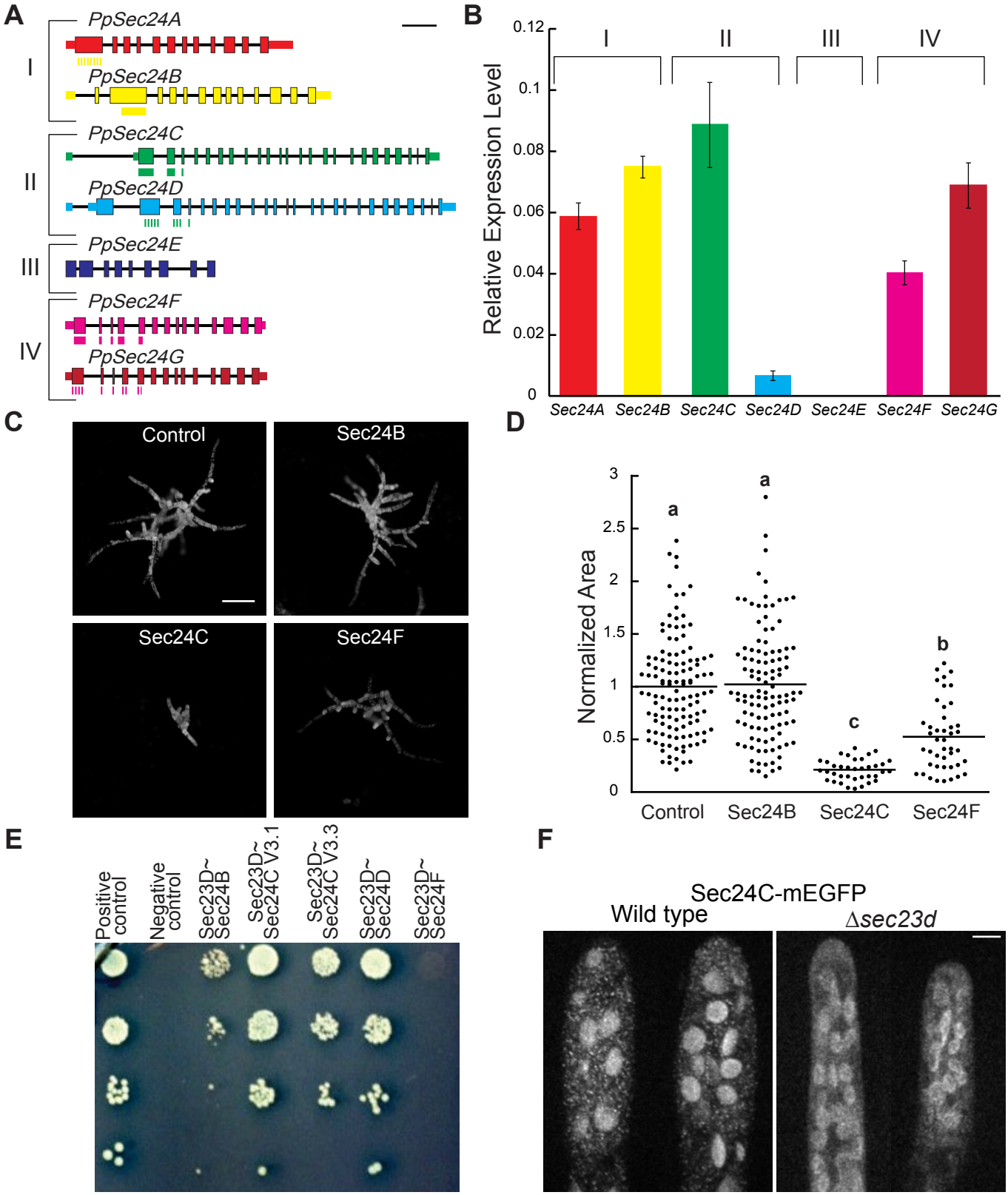

Figure 7. *Sec24* isoforms differentially contribute to protonemal growth. (A) *Sec24* gene models are shown with exons indicated by boxes and introns by thin black lines. Coding and untranslated regions are denoted by thick and thin boxes, respectively. Lines underneath the models represent sequence regions that were targeted by Sec24 RNAi constructs. Scale bar, 1000 bp. (B) Relative expression of *Sec24* genes normalized to UBIQUITIN10 in 8-day-old wild-type moss plants regenerated from protoplasts. N=3, Error bars are s.e.m. (C) Representative chlorophyll autofluorescence images of 7-day old plants regenerated from protoplasts expressing the indicated RNAi constructs. Scale bar, 100 µm. (D) Quantification of plant area is based on the area of the chlorophyll autofluorescence and is presented normalized to the area of the control. Means are indicated by horizontal lines. Letters indicate groups with significantly different means as determined by a one-way ANOVA with a Tukey *post hoc* test (α=0.05). (E) Serial dilutions of yeast strains carrying 2-hybrid vectors testing for interaction between Sec23D and the indicated Sec24 isoforms. Growth indicates that tested proteins interact. *Sec24C* V3.1 and V3.3 are two splice variants isolated from 7-day old protonemal tissue. Positive control: murine p53 insert and SV40 large T-antigen; Negative control: human lamin and SV40 large T-antigen (Clontech). (F) Representative maximum projections of confocal images of endogenously tagged Sec24C-mEGFP in the indicated genotypes. Large globular structures are chloroplasts, which autofluoresce under these imaging conditions. Scale bar, 5 µm.

Parsed Citations

Aridor, M. (2018). COPII gets in shape: Lessons derived from morphological aspects of early secretion. Traffic 19: 823–839.
Pubmed: Author and Title
Google Scholar: Author Only Title Only Author and Title

Aridor, M., Fish, K.N., Bannykh, S., Weissman, J., Roberts, T.H., Lippincott-Schwartz, J., and Balch, W.E. (2001). The Sar1 Gtpase Coordinates Biosynthetic Cargo Selection with Endoplasmic Reticulum Export Site Assembly. Journal of Cell Biology 152: 213–230.
Pubmed: Author and Title
Google Scholar: Author Only Title Only Author and Title

Aridor, M., Weissman, J., Bannykh, S., Nuoffer, C., and Balch, W.E. (1998). Cargo Selection by the COPII Budding Machinery during Export from the ER. Journal of Cell Biology 141: 61–70.
Pubmed: Author and Title
Google Scholar: Author Only Title Only Author and Title

Augustine, R.C., Pattavina, K.A., Tüzel, E., Vidali, L., and Bezanilla, M. (2011). Actin interacting protein1 and actin depolymerizing factor drive rapid actin dynamics in Physcomitrella patens. Plant Cell 23: 3696–3710.
Pubmed: Author and Title
Google Scholar: Author Only Title Only Author and Title

Barlow, L.D. and Dacks, J.B. (2018). Seeing the endomembrane system for the trees: Evolutionary analysis highlights the importance of plants as models for eukaryotic membrane-trafficking. Seminars in Cell & Developmental Biology 80: 142–152.
Pubmed: Author and Title
Google Scholar: Author Only Title Only Author and Title

Barlowe, C. (2003). Signals for COPII-dependent export from the ER: what's the ticket out? Trends in Cell Biology 13: 295–300.
Pubmed: Author and Title
Google Scholar: Author Only Title Only Author and Title

Barlowe, C. and Helenius, A. (2016). Cargo Capture and Bulk Flow in the Early Secretory Pathway. Annu. Rev. Cell Dev. Biol. 32: 197–222.
Pubmed: Author and Title
Google Scholar: Author Only Title Only Author and Title

Barlowe, C. and Schekman, R. (1993). SEC12 encodes a guanine-nucleotide-exchange factor essential for transport vesicle budding from the ER. Nature 365: 347–349.
Pubmed: Author and Title
Google Scholar: Author Only Title Only Author and Title

Bascom, C.S., Wu, S.-Z., Nelson, K., Oakey, J., and Bezanilla, M. (2016). Long-Term Growth of Moss in Microfluidic Devices Enables Subcellular Studies in Development. Plant Physiology 172: 28–37.
Pubmed: Author and Title
Google Scholar: Author Only Title Only Author and Title

Bascom Jr, C., Burkart, G.M., Mallett, D.R., O'Sullivan, J.E., Tomaszewski, A.J., Walsh, K., and Bezanilla, M. (2018). Systematic survey of the function of ROP regulators and effectors during tip growth in the moss Physcomitrella patens. J. Exp. Bot. 70: 447–457.
Pubmed: Author and Title
Google Scholar: Author Only Title Only Author and Title

Belden, W.J. (2001). Role of Erv29p in Collecting Soluble Secretory Proteins into ER-Derived Transport Vesicles. Science 294: 1528–1531.
Pubmed: Author and Title
Google Scholar: Author Only Title Only Author and Title

Bezanilla, M., Perroud, P.-F., Pan, A., Klueh, P., and Quatrano, R.S. (2005). An RNAi system in Physcomitrella patens with an internal marker for silencing allows for rapid identification of loss of function phenotypes. Plant Biol (Stuttg) 7: 251–257.
Pubmed: Author and Title
Google Scholar: Author Only Title Only Author and Title

Bi, X., Corpina, R.A., and Goldberg, J. (2002). Structure of the Sec23/24–Sar1 pre-budding complex of the COPII vesicle coat. Nature 419: 271–277.
Pubmed: Author and Title
Google Scholar: Author Only Title Only Author and Title

Brandizzi, F. (2018). Transport from the endoplasmic reticulum to the Golgi in plants: Where are we now? Seminars in Cell & Developmental Biology 80: 94–105.
Pubmed: Author and Title
Google Scholar: Author Only Title Only Author and Title

Brandizzi, F. and Barlowe, C. (2013). Organization of the ER–Golgi interface for membrane traffic control. Nat Rev Mol Cell Biol 14: 382–392.
Pubmed: Author and Title
Google Scholar: Author Only Title Only Author and Title

Cho, Y. and Kanehara, K. (2017). Endoplasmic Reticulum Stress Response in Arabidopsis Roots. Front. Plant Sci. 8.
Pubmed: Author and Title
Google Scholar: Author Only Title Only Author and Title

Chung, K.P., Zeng, Y., and Jiang, L. (2016). COPII Paralogs in Plants: Functional Redundancy or Diversity? Trends in Plant Science 21: 758–769.
Pubmed: Author and Title
Google Scholar: Author Only Title Only Author and Title

De Craene, J.-O., Courte, F., Rinaldi, B., Fitterer, C., Herranz, M.C., Schmitt-Keichinger, C., Ritzenthaler, C., and Friant, S. (2014). Study of the Plant COPII Vesicle Coat Subunits by Functional Complementation of Yeast Saccharomyces cerevisiae Mutants. PLoS ONE 9: e90072.
Pubmed: Author and Title
Google Scholar: Author Only Title Only Author and Title

Faso, C., Chen, Y.-N., Tamura, K., Held, M., Zemelis, S., Marti, L., Saravanan, R., Hummel, E., Kung, L., Miller, E., Hawes, C., and Brandizzi, F. (2009). A Missense Mutation in the Arabidopsis COPII Coat Protein Sec24A Induces the Formation of Clusters of the Endoplasmic Reticulum and Golgi Apparatus. The Plant Cell 21: 3655–3671.
Pubmed: Author and Title
Google Scholar: Author Only Title Only Author and Title

Fath, S., Mancias, J.D., Bi, X., and Goldberg, J. (2007). Structure and Organization of Coat Proteins in the COPII Cage. Cell 129: 1325–1336.
Pubmed: Author and Title
Google Scholar: Author Only Title Only Author and Title

Furt, F., Lemoi, K., Tüzel, E., and Vidali, L. (2012). Quantitative analysis of organelle distribution and dynamics in Physcomitrella patens protonemal cells. BMC Plant Biol. 12: 70.
Pubmed: Author and Title
Google Scholar: Author Only Title Only Author and Title

Galotto, G., Bibeau, J.P., and Vidali, L. (2019). Automated Image Acquisition and Morphological Analysis of Cell Growth Mutants in Physcomitrella patens. In Plant Cell Morphogenesis, F. Cvrčková and V. Žárský, eds, Methods in Molecular Biology. (Springer New York: New York, NY), pp. 307–322.
Pubmed: Author and Title
Google Scholar: Author Only Title Only Author and Title

Giraudo, C.G. and Maccioni, H.J.F. (2003). Endoplasmic Reticulum Export of Glycosyltransferases Depends on Interaction of a Cytoplasmic Dibasic Motif with Sar1. MBoC 14: 3753–3766.
Pubmed: Author and Title
Google Scholar: Author Only Title Only Author and Title

van Gisbergen, P.A.C., Wu, S.-Z., Chang, M., Pattavina, K.A., Bartlett, M.E., and Bezanilla, M. (2018). An ancient Sec10-formin fusion provides insights into actin-mediated regulation of exocytosis. J. Cell Biol. 217: 945–957.
Pubmed: Author and Title
Google Scholar: Author Only Title Only Author and Title

Haeussler, M., Schönig, K., Eckert, H., Eschstruth, A., Mianné, J., Renaud, J.-B., Schneider-Maunoury, S., Shkumatava, A., Teboul, L., Kent, J., Joly, J.-S., and Concordet, J.-P. (2016). Evaluation of off-target and on-target scoring algorithms and integration into the guide RNA selection tool CRISPOR. Genome Biol. 17: 148.
Pubmed: Author and Title
Google Scholar: Author Only Title Only Author and Title

Hanna, M.G., Peotter, J.L., Frankel, E.B., and Audhya, A. (2018). Membrane Transport at an Organelle Interface in the Early Secretory Pathway: Take Your Coat Off and Stay a While: Evolution of the metazoan early secretory pathway. BioEssays 40: 1800004.
Pubmed: Author and Title
Google Scholar: Author Only Title Only Author and Title

Hanton, S.L., Matheson, L.A., Chatre, L., and Brandizzi, F. (2009). Dynamic organization of COPII coat proteins at endoplasmic reticulum export sites in plant cells. The Plant Journal 57: 963–974.
Pubmed: Author and Title
Google Scholar: Author Only Title Only Author and Title

Hino, T., Tanaka, Y., Kawamukai, M., Nishimura, K., Mano, S., and Nakagawa, T. (2011). Two Sec13p Homologs, AtSec13A and AtSec13B, Redundantly Contribute to the Formation of COPII Transport Vesicles in Arabidopsis thaliana. Bioscience, Biotechnology, and Biochemistry 75: 1848–1852.
Pubmed: Author and Title
Google Scholar: Author Only Title Only Author and Title

Jensen, D. and Schekman, R. (2011). COPII-mediated vesicle formation at a glance. Journal of Cell Science 124: 1–4.
Pubmed: Author and Title
Google Scholar: Author Only Title Only Author and Title

Khoriaty, R. et al. (2018). Functions of the COPII gene paralogs SEC23A and SEC23B are interchangeable in vivo. Proc Natl Acad Sci

USA 115: E7748–E7757.
Pubmed: Author and Title
Google Scholar: Author Only Title Only Author and Title

Lee, M.H., Lee, S.H., Kim, H., Jin, J.B., Kim, D.H., and Hwang, I. A WD40 Repeat Protein, Arabidopsis Sec13 Homolog 1, May Play a Role in Vacuolar Trafficking by Controlling the Membrane Association of AtDRP2A: 10.

Mallett, D.R., Chang, M., Cheng, X., and Bezanilla, M. (2019). Efficient and modular CRISPR-Cas9 vector system for Physcomitrella patens. Plant Direct 3: e00168-15.
Pubmed: Author and Title
Google Scholar: Author Only Title Only Author and Title

Mancias, J.D. and Goldberg, J. (2007). The Transport Signal on Sec22 for Packaging into COPII-Coated Vesicles Is a Conformational Epitope. Molecular Cell 26: 403–414.
Pubmed: Author and Title
Google Scholar: Author Only Title Only Author and Title

Maruyama, D., Sugiyama, T., Endo, T., and Nishikawa, S. (2014). Multiple BiP Genes of Arabidopsis thaliana are Required for Male Gametogenesis and Pollen Competitiveness. Plant and Cell Physiology 55: 801–810.
Pubmed: Author and Title
Google Scholar: Author Only Title Only Author and Title

Mossessova, E., Bickford, L.C., and Goldberg, J. (2003). SNARE selectivity of the COPII coat. Cell 114: 483–495.
Pubmed: Author and Title
Google Scholar: Author Only Title Only Author and Title

Nakano, A. and Muramatsu, M. (1989). A Novel GTP-binding Protein, Sar1p, Is Involved in Transport from the Endoplasmic Reticulum to the Golgi Apparatus. The Journal of Cell Biology 109: 2677–2691.
Pubmed: Author and Title
Google Scholar: Author Only Title Only Author and Title

Nakano, R.T., Matsushima, R., Ueda, H., Tamura, K., Shimada, T., Li, L., Hayashi, Y., Kondo, M., Nishimura, M., and Hara-Nishimura, I. (2009). GNOM-LIKE1/ERMO1 and SEC24a/ERMO2 Are Required for Maintenance of Endoplasmic Reticulum Morphology in Arabidopsis thaliana. The Plant Cell 21: 3672–3685.
Pubmed: Author and Title
Google Scholar: Author Only Title Only Author and Title

Nebenfuhr, A. (2002). Brefeldin A: Deciphering an Enigmatic Inhibitor of Secretion. Plant physiology 130: 1102–1108.
Pubmed: Author and Title
Google Scholar: Author Only Title Only Author and Title

Nelson, B.K., Cai, X., and Nebenführ, A. (2007). A multicolored set of in vivo organelle markers for co-localization studies in Arabidopsis and other plants. Plant J. 51: 1126–1136.
Pubmed: Author and Title
Google Scholar: Author Only Title Only Author and Title

Niu, T.-K., Pfeifer, A.C., Lippincott-Schwartz, J., and Jackson, C.L. (2005). Dynamics of GBF1, a Brefeldin A-Sensitive Arf1 Exchange Factor at the Golgi□V. Molecular Biology of the Cell 16: 1213–1222.
Pubmed: Author and Title
Google Scholar: Author Only Title Only Author and Title

Noh, S.-J., Kwon, C.S., Oh, D.-H., Moon, J.S., and Chung, W.-I. (2003). Expression of an evolutionarily distinct novel BiP gene during the unfolded protein response in Arabidopsis thaliana. Gene 311: 81–91.
Pubmed: Author and Title
Google Scholar: Author Only Title Only Author and Title

Novick, P., Field, C., and Schekman, R. (1980). Identification of 23 complementation groups required for post-translational events in the yeast secretory pathway. Cell 21: 205–215.
Pubmed: Author and Title
Google Scholar: Author Only Title Only Author and Title

Nufer, O. (2003). ER export of ERGIC-53 is controlled by cooperation of targeting determinants in all three of its domains. Journal of Cell Science 116: 4429–4440.
Pubmed: Author and Title
Google Scholar: Author Only Title Only Author and Title

Ortiz-Ramírez, C., Michard, E., Simon, A.A., Damineli, D.S.C., Hernandez-Coronado, M., Becker, J.D., and Feijó, J.A. (2017). GLUTAMATE RECEPTOR-LIKE channels are essential for chemotaxis and reproduction in mosses. Nature 549: 91–95.
Pubmed: Author and Title
Google Scholar: Author Only Title Only Author and Title

Qu, X., Zhang, R., Zhang, M., Diao, M., Xue, Y., and Huang, S. (2017). Organizational innovation of apical actin filaments drives rapid pollen tube growth and turning. Mol Plant 10: 930–947.
Pubmed: Author and Title
Google Scholar: Author Only Title Only Author and Title

Rensing, S.A., Goffinet, B., Meyberg, R., Wu, S.-Z., and Bezanilla, M. (2020). The Moss Physcomitrium (Physcomitrella) patens : A Model Organism for Non-Seed Plants. Plant Cell 32: 1361–1376.
Pubmed: Author and Title
Google Scholar: Author Only Title Only Author and Title

Salama, N.R., Yeung, T., and Schekman, R.W. The Sec13p complex and reconstitution of vesicle budding from the ER with purified cytosolic proteins. The EMBO Journal 12: 4073–4082.
Pubmed: Author and Title
Google Scholar: Author Only Title Only Author and Title

Srivastava, R., Deng, Y., Shah, S., Rao, A.G., and Howell, S.H. (2013). BINDING PROTEIN Is a Master Regulator of the Endoplasmic Reticulum Stress Sensor/Transducer bZIP28 in Arabidopsis. Plant Cell 25: 1416–1429.
Pubmed: Author and Title
Google Scholar: Author Only Title Only Author and Title

Stagg, S.M., Gürkan, C., Fowler, D.M., LaPointe, P., Foss, T.R., Potter, C.S., Carragher, B., and Balch, W.E. (2006). Structure of the Sec13/31 COPII coat cage. Nature 439: 234–238.
Pubmed: Author and Title
Google Scholar: Author Only Title Only Author and Title

Stagg, S.M., LaPointe, P., Razvi, A., Gürkan, C., Potter, C.S., Carragher, B., and Balch, W.E. (2008). Structural Basis for Cargo Regulation of COPII Coat Assembly. Cell 134: 474–484.
Pubmed: Author and Title
Google Scholar: Author Only Title Only Author and Title

Takagi, J., Renna, L., Takahashi, H., Koumoto, Y., Tamura, K., Stefano, G., Fukao, Y., Kondo, M., Nishimura, M., Shimada, T., Brandizzi, F., and Hara-Nishimura, I. (2013). MAIGO5 Functions in Protein Export from Golgi-Associated Endoplasmic Reticulum Exit Sites in Arabidopsis. The Plant Cell 25: 4658–4675.
Pubmed: Author and Title
Google Scholar: Author Only Title Only Author and Title

Tanaka, Y., Nishimura, K., Kawamukai, M., Oshima, A., and Nakagawa, T. (2013). Redundant function of two Arabidopsis COPII components, AtSec24B and AtSec24C, is essential for male and female gametogenesis. Planta 238: 561–575.
Pubmed: Author and Title
Google Scholar: Author Only Title Only Author and Title

Vidali, L., Augustine, R.C., Kleinman, K.P., and Bezanilla, M. (2007). Profilin is essential for tip growth in the moss Physcomitrella patens. Plant Cell 19: 3705–3722.
Pubmed: Author and Title
Google Scholar: Author Only Title Only Author and Title

Vidali, L., van Gisbergen, P.A.C., Guérin, C., Franco, P., Li, M., Burkart, G.M., Augustine, R.C., Blanchoin, L., and Bezanilla, M. (2009). Rapid formin-mediated actin-filament elongation is essential for polarized plant cell growth. Proc. Natl. Acad. Sci. U.S.A. 106: 13341–13346.
Pubmed: Author and Title
Google Scholar: Author Only Title Only Author and Title

Viotti, C. et al. (2013). The Endoplasmic Reticulum Is the Main Membrane Source for Biogenesis of the Lytic Vacuole in Arabidopsis. Plant Cell 25: 3434–3449.
Pubmed: Author and Title
Google Scholar: Author Only Title Only Author and Title

Whittle, J.R.R. and Schwartz, T.U. (2010). Structure of the Sec13–Sec16 edge element, a template for assembly of the COPII vesicle coat. The Journal of Cell Biology 190: 347–361.
Pubmed: Author and Title
Google Scholar: Author Only Title Only Author and Title

Wu, S.-Z. and Bezanilla, M. (2014). Myosin VIII associates with microtubule ends and together with actin plays a role in guiding plant cell division. eLife Sciences 3: e03498.
Pubmed: Author and Title
Google Scholar: Author Only Title Only Author and Title

Zeng, Y., Chung, K.P., Li, B., Lai, C.M., Lam, S.K., Wang, X., Cui, Y., Gao, C., Luo, M., Wong, K.-B., Schekman, R., and Jiang, L. (2015). Unique COPII component AtSar1a/AtSec23a pair is required for the distinct function of protein ER export in Arabidopsis thaliana. Proc Natl Acad Sci USA 112: 14360–14365.
Pubmed: Author and Title
Google Scholar: Author Only Title Only Author and Title